POSITRON ANNIHILATION INVESTIGATION OF ELECTRON IRRADIATED SILICON

By

VICTOR P. AVALOS

A Thesis
Submitted to the Faculty of Graduate Studies
in Partial Fulfillment of the Requirements
for the Degree of

MASTER OF SCIENCE

Department of Physics
University of Manitoba
Winnipeg, Manitoba

THE UNIVERSITY OF MANITOBA

FACULTY OF GRADUATE STUDIES

*****

COPYRIGHT PERMISSION PAGE

POSITRON ANNIHILATION INVESTIGATION OF ELECTRON IRRADIATED SILICON

BY

VICTOR P. AVALOS

A Thesis/Practicum submitted to the Faculty of Graduate Studies of The University of Manitoba in partial fulfillment of the requirements of the degree of

MASTER OF SCIENCE

TABLE OF CONTENTS:

ABSTRACT:

Positron annihilation experiments which combine lifetime and doppler broadening measurements were performed using 10 MeV electron-irradiated Float-zone (Fz) and Czochralski silicon (Cz).

In the case of irradiated float-zone Si, a lifetime of 305 ps is observed at 300 K decreasing from 290 ps at 30 K, and the positron trapping rate decreases strongly with increasing temperature. The Doppler measurements yield, when coupled with lifetime data, a S-value 6.7% larger than that for the bulk which is nearly twice the value hitherto claimed for divacancies. Isochronal annealing of the 1.8 μm infrared absorption band is accompanied by a significant change in the defect S-value to 3.8% larger than for the bulk. Surprisingly, the trapping rate at 50 K decreases only by 30% during the annealing-out of the 1.8 μm infrared absorption, and the positron lifetime stays essentially constant. Loose vacancy complexes (a "sponge" defect) consisting of discernible monovacancies are suggested to be formed upon annealing as an intermediate step in clustering of divacancies.

For the Cz-silicon, a set of rectangular wafers of n-type (P, Sb doped) and p-type (B doped) at various concentration levels and irradiated to a fluence of $1.2x10^{18}e^{-}/cm^{2}$ were investigated as a function of temperature and position dependence. The low dopant concentration samples of p-type or n-type present a dominance of negative divacancy defects, due to a lifetime of ~300 ps, a strong temperature dependence of the trapping rate and a S_D/S_B value 1.07. For the middle concentration materials, we proposed that the formation of neutral PV_2, BV_2 and SbV_2 type defects would explain the strong temperature dependence of the lifetime while maintaining constant trapping rate. In the highly doped n-or-p-type samples (both with $5x10^{18}/cm^{3}$), the n-type (P-doped) shows a dominance of VP pairs, which are stable at room temperature, while for the p-type (B doped) we suggest the BV_2 are present given that VB is unstable at room temperature.

ACKNOWLEDGEMENTS

The work presented in this report was carried out in partial fulfilment of the requirements for obtaining the MASTER IN SCIENCE degree from the University of Manitoba, Canada. This work was carried out at the Positron Laboratory of the Physics Department of the University of Winnipeg, Canada under the supervision of professor Steen Dannefaer.

I am very grateful to professor Dannefaer, who enabled me to carry out the research reported in this thesis, and especially for his constructive advise and guidance which I always found very helpful to me.

I am especially grateful to my wife, Nelly, for the continuous support that she has given me through all these years.

And finally, I am very thankful to my Heavenly Father who has given me the wisdom and strength to complete this work . "The Lord giveth wisdom: out of his mouth cometh knowledge and undestanding" Prov. 2:6.

CHAPTER ONE

INTRODUCTION

1.1 INTRODUCTION:

We like to admire the real thing, thus we commonly prefer pure wool, sugar, gold etc. There are instances where because of cost, availability or properties its more desirable to have impurities present. For example, sterling silver contains 7.5% copper and 92.5% silver or in the case of zinc which when added to copper produces brass, at a lower cost than pure copper but stronger, harder, and more ductile than pure copper. On the other hand brass has lower electrical conductivity than copper. A similar situation happens with iron where carbon, nickel, chromium, vanadium etc. can be added so to improve the mechanical properties of pure iron. Therefore, it can be seen that by adding impurities to some materials their mechanical and electrical properties can be changed beneficially.

The addition of impurities to semiconducting materials such as silicon (Si) or germanium (Ge) has produced results that have revolutionized today's world of technology. The physics behind why this happens is the main reason why many scientists have devoted a great deal of time and industry financial resources, to find out in as much detail as possible, about this phenomenon. In this pursuit many branches and fields of research have been developed, and because this research is at the atomic level, many sophisticated methods have been designed to accomplish this work. One of these methods of research is the positron annihilation technique on which I will concentrate in this work.

1.2 HISTORICAL INTRODUCTION TO POSITRON ANNIHILATION:

In 1926 Gordon and Klein [1] had formulated the relativistic quantum mechanical theory, from which emerged the possibility of negative energies for the electron. Also in 1926, P.A.M. Dirac [2] removed the dependence on time of the Gordon Klein equations in a non-linear way, but the problem of negative energies for electrons still existed in Dirac's equation. Dirac tried to explain them by associating them with the properties of the proton, the only positive elementary particle known at that time. But he realized that the solution had to be connected with particles with a mass like that of an electron. In 1930 Dirac published "Theory of Electrons and Protons" [3] where he postulated his famous "Holes" theory, predicting the existence of a positive electron. In his theory, the positron was viewed as a missing electron in a sea of electrons all with negative energy. In the years around 1930, investigations were carried out using the Wilson chambers in order to study the different reactions which high-energy cosmic radiation might undergo with matter. In the presence of strong magnetic fields, trajectories of particles are curved oppositely depending on the charge of the particles. In 1932, after a careful analysis of a photographic plate, Anderson [4,5] came to the conclusion that the tracks observed must originate from positive particles, the mass of which is closer to that of an electron than to that of a proton. These observations were purely experimental, and Anderson did not know about the theory of Dirac. Not until 1933, in a paper published by Blackett and Occhialini [6], was it

demonstrated that the experimentally observed properties of the new particle were those predicted by Dirac's theory.

As shown in Dirac's theory when positrons and electrons are in near proximity, for even a very short period of time, they annihilate each other emitting as γ–quanta the energy:

$$E = 2m_oc^2 + E_+ + E_- \qquad (1.1)$$

where m_oc^2 is the rest mass energy of an electron or positron and E_+ and E_- are the kinetic energies of the electron and positron.

In 1934, Thibaud [7] showed that the positron annihilates predominantly by the emission of 2 γ-quanta, each with an energy of 0.511 MeV, corresponding to the rest-mass energy of e^- or e^+ and also that certain radioactive sources emitted positrons. (In rare cases, 1:372, 3γ-rays could be emitted). Later Klemperer [8] demonstrated that the 2 γ-quanta were emitted in coincidence and in almost opposite directions in order to conserve momentum. The deviation ,θ, from the angle of 180° is determined by:

$$\theta = p/m_oc \qquad (1.2)$$

where p is the total momentum of the annihilating pair perpendicular to the direction of photon emission, c the speed of light and m_0 the electron rest mass.

1.3 ANNIHILATION OF POSITRONS:

When the positron enters the material from a radioactive source, the kinetic energy is rather high (several hundreds of keV depending on the source), and this energy is lost by colli-

sions with the atoms of the material. This slow-down process normally takes about 10^{-12} to 10^{-14} seconds in solids, whereas in gases it may take several nanoseconds. Only a very small fraction of the positrons annihilates during the slow-down time due to its shortness as compared to the lifetime of the positrons. Thus, effectively first when the positron is thermalized, annihilation can take place with electrons. It may annihilate as a free (delocalized) particle or as a defect in a solid, or it may annihilate from a state where it is bound to one electron only; this bound state is called positronium.

It is this very diversity in the annihilation processes of the positron which make them a useful tool in, for example, defect detection.

1.3.1 POSITRONIUM:

The positronium atom (Ps) is a bound state of an electron and a positron. It is an analogue of the hydrogen atom, only that the proton is replaced by the positron. This means that it is treated in lowest order as a hydrogen atom with a reduced mass of $m_e/2$. The binding energy in the ground state will be half of that of a hydrogen atom, i.e. E_B=6.8 eV. The radius in the relative movement of the electron and positron is double of the Bohr radius, resulting in a diameter of the positronium atom like that of a hydrogen atom, 1.06 Å. The positronium ground state splits into two different states, the singlet ($^1S_0$) or para state (p-Ps), where the spins of the electron and positron are antiparallel. This gives for the angular momentum the quantum numbers J=0 and m=0. The second state is the triplet ($^3S_1$), or ortho

state (o-Ps), where the spins of the electron and positron are parallel; this state has J=1 and is divided into three degenerate substates with m=-1,0,+1.

Having zero spin, p-Ps undergoes mainly 2γ-annhihilation. For free p-Ps, the lifetime is 1.25×10^{-10} sec (125 ps) [9]. The free o-Ps on the other hand can only undergo 3 γ-annihilation (in order to conserve spin) with a lifetime of about 1.4×10^{-7} sec (140 ns) [9]. The energy difference between the two states is only 8×10^{-3}eV. For this reason, one quarter of the formed positronium is in the singlet state and the other three quarters are in the triplet state as dictated by occupation statistics.

The subject dealt with in this section is treated in more detail in references [10] and [11].

CHAPTER TWO

INTRODUCTION TO EXPERIMENTAL TECHNIQUES

2.1 INTRODUCTION TO EXPERIMENTAL TECHNIQUES:

At this point a general overview is given of the three methods normally used to extract the information carried by the annihilation quanta as shown in figure 2.1 [8].

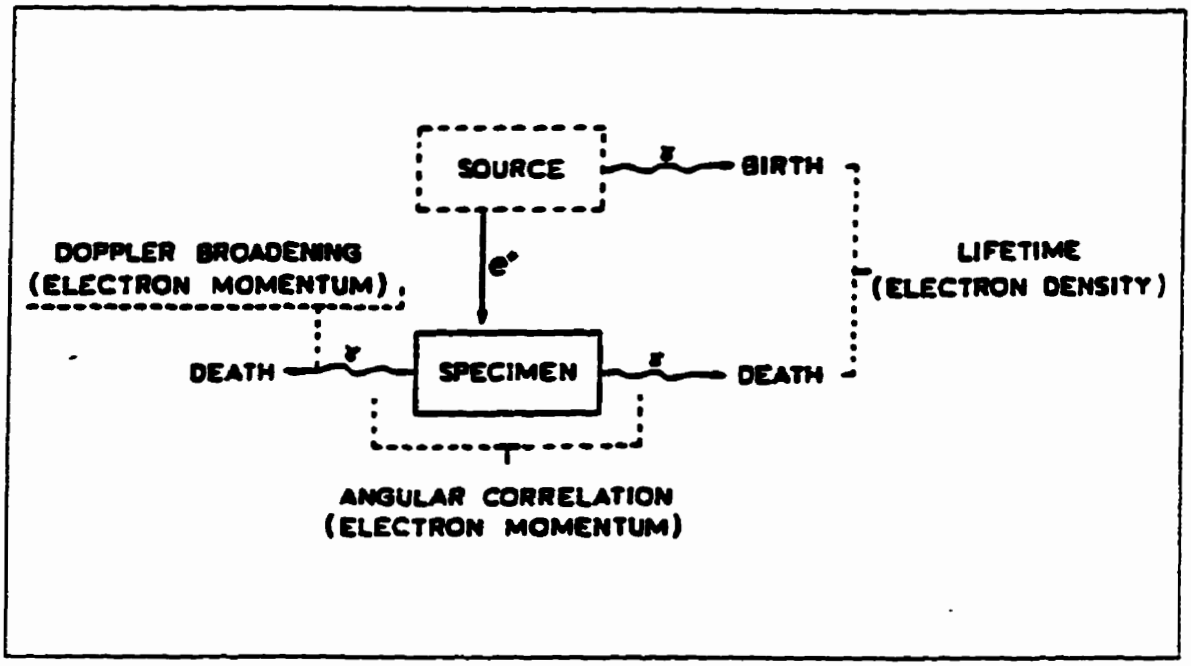

Figure 2.1. Representation of methods used to extract the information obtained by the annihilation quanta.

Measurement of positron lifetime gives information about electron density, while measurement of angular correlation between the two annihilation quanta or measurements of the Doppler shift of one of the quanta, gives information about electron momenta.

In all experimental techniques described here, a radioactive material emitting positrons is used as a positron source. The most commonly used is ^{22}Na (in the form of $^{22}NaCl$), which has a half life of 2.6 years; its decay scheme is shown in figure 2.2.

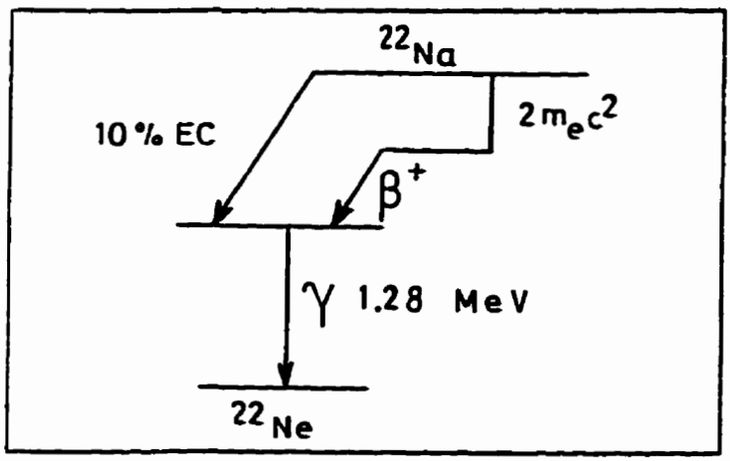

Figure 2.2. Decay scheme of Na^{22}.

2.2. SLOW-DOWN AND THERMALIZATION:

In positron annihilation studies, positrons are implanted into the sample with kinetic energies according to a β^+ energy spectrum whose end point energy is about 0.54 keV and thus exceeds considerably the thermal energy k_BT. After implantation, the positron loses its energy due to electron and phonon excitation.

The stopping profile of energetic positrons from a radioactive source is exponential, and is given by:

$$P(x) = \alpha e^{-\alpha x} \text{ with } \alpha = (16\rho(g/cm^3))/E_{max}^{1.4}(Mev) \qquad (2.1)$$

where ρ is the density of the solid and E_{max} the maximum energy of the emitted positrons. The most common isotope for positron lifetime and Doppler broadening experiments is ^{22}Na with E_{max}=0.54 MeV. For this isotope the average penetration depth, $1/\alpha$, is 0.11 mm in silicon for which reason positrons emitted from a radioactive source probe the bulk of the solid.

In a solid, energetic positrons rapidly loose their energy via ionization and core electrons excitations. The energy-loss rate in the range of 1 MeV >E_+>100 keV is about 1 MeV/ps, and from 100 keV to 100 eV it is 100 keV/ps. Below 1 eV, phonon excitation starts to be noticeable. The thermalization time at 300 K is 1-3 ps, which is much less than a typical positron lifetime of more than 100 ps. Even at 10 K, calculated thermalization times are much less than positron lifetimes .

In semiconductors, electron excitations are not possible when the kinetic energy of the positrons is less than the band gap energy E_g. However, energy loss to phonons is quite effective at $E_+ \approx 1$ eV.

In conclusion, positrons from a radioactive source probe the bulk of a sample. The thermalization time for positrons in metals and semiconductors is short, compared to positron lifetime, and is not of experimental concern

2.3. ANGULAR CORRELATION TECHNIQUE:

A schematic set up for an angular correlation equipment is shown in figure 2.3. The angular correlation between 2γ annihilation quanta is measured. The distance from the sample to the two detectors is usually about 2 meters. One detector is fixed while the other can be turned by a small (<20 mrad.) angle, θ, and the number of incident photons is measured as a function of θ. After amplification of the detector pulses, they are analyzed for the correct energy (0.51 MeV) and then fed into a coincidence circuit, giving an output

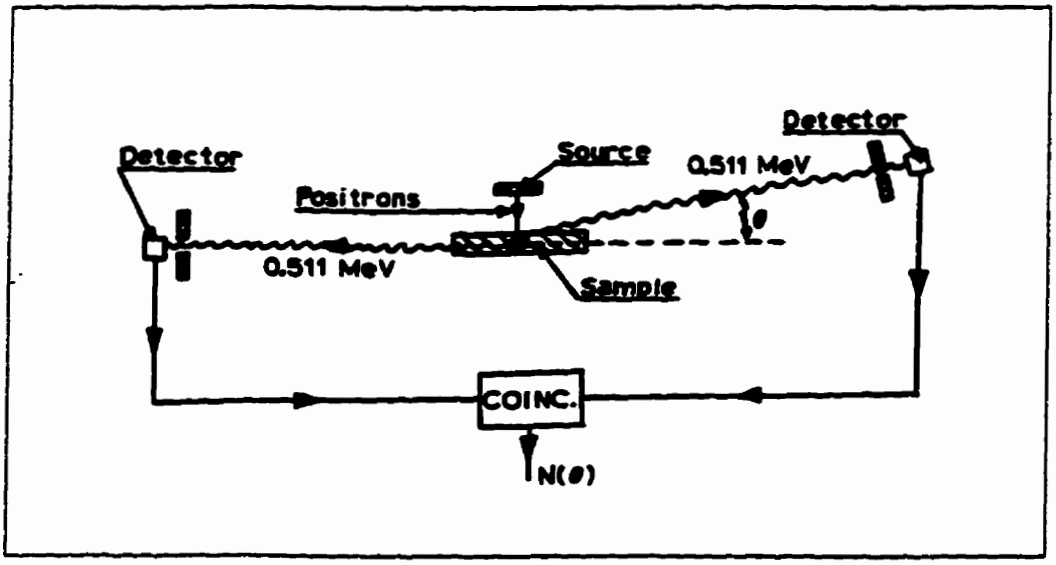

Figure 2.3 Principle of typical angular correlation equipment

if the time difference is smaller than 100 ns. As already noticed, momentum conservation of the annihilation pair with center-of-mass momentum k, requires a deviation from 180° between the two quanta, a deviation largely due to electron momentum as the positron is thermalized. By the long slit geometry this deviation is measured only in the direction of the movement of the one detector, the z direction and by the movement of the detector in stepwise way, the rate of coincidence pulses is measured as a function of θ_z giving as a result the angular correlation curved shown schematically in figure 2.4.

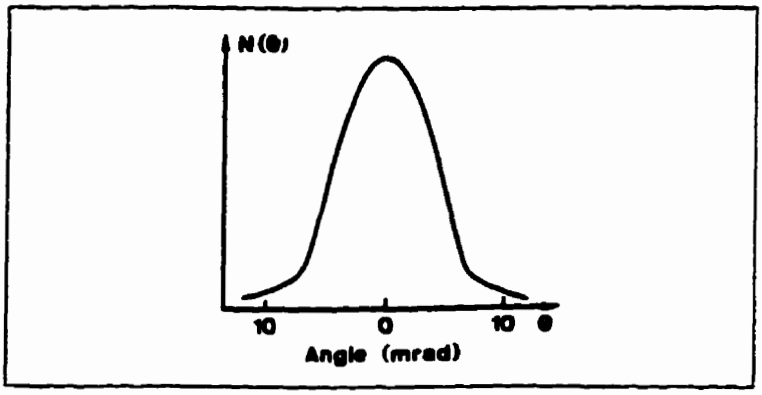

Figure 2.4 Typical angular correlation curve

Angular correlation measurements provide information on the momentum distribution of electrons and can thus be used for Fermi-surface studies. In cases of Ps formation, the angular correlation measurements will show a very narrow peak due to the low momentum spread of thermalized p-Ps.

2.4 DOPPLER BROADENING:

In Doppler broadening measurement the energy spread of the annihilation quanta is determined. In principle Doppler measurements and angular correlation measurements provide identical information, but the resolution power of Doppler broadening is about 5 times less than that of angular correlation. The speed of the data aquisition for Doppler brodening is on the other hand at least 10 times faster than for angular correlation, which takes at least 24 hours per spectrum.

The velocity component $V_{cm,x}$ (center of mass) of the annihilating electron-positron pair, as projected onto the direction of the emitted γ-quanta, leads to a Doppler shift of the energy of the γ quantum. The energies E_1 and E_2, depend on wheather $V_{cm,x}$ is directed opposite to the direction of the emitted γ-ray, or along the direction according to:

$$E_{1,2}=m_oc^2\{(1\pm V_{cm,x}/c)/(1-V_{cm}^2/c^2)^{0.5}\} \qquad (2.4)$$

which for $V_{cm,x}<<c$ simplifies to

$$E_{1,2} \approx m_0c^2 \pm p_xc/2 \qquad (2.5)$$

or expressed in relative energy difference

$$\Delta E/E_0 = \pm V_{cm}/c \quad \text{where } V_{cm} = V_{electron}/2 \qquad (2.6)$$

Those small energy changes (of the order of a few keV) are measurable with an energy sensitive Ge detector system, for which a schematic is shown in figure 2.5 [14]. The resolution of a Ge detector is rather poor in comparison with an angular correlation equipment. The best detectors have a resolution function of approximately 1.2 keV (≈5 mrad.) which is rather inferior to what can be achieved by angular correlation (less than 1 mrad). The system has, however, the advantage of a high counting rate and good statistics.

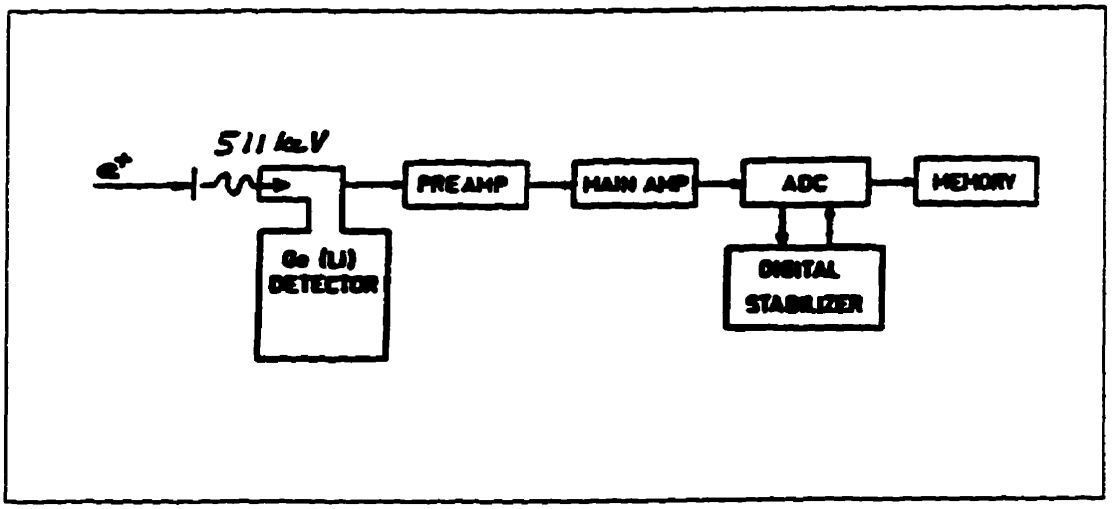

Figure 2.5. Typical equipment used in measuring the doppler shifts of the annihilation quanta.

2.4.1 THE S AND W PARAMETERS:

Analysis of the Doppler broadening data is normally restricted to rather simple approaches because of the wide resolution. The width of the 511 keV peak is characterized by a so-

called S parameter as introduced by MacKenzie et al [15]. This S parameter is defined as the ratio between the amount of counts in the central region of the annihilation line, normally within the energy range 511±0.7 keV, to the total number in the peak within 511±4.8 keV, as shown in figure 2.6. This "window" of energy is usually chosen so that S≈0.5 [16]. In the same way, the wing parameter W, shown in figure 2.6, is the relative fraction of the counts in the wing regions of the annihilation line.

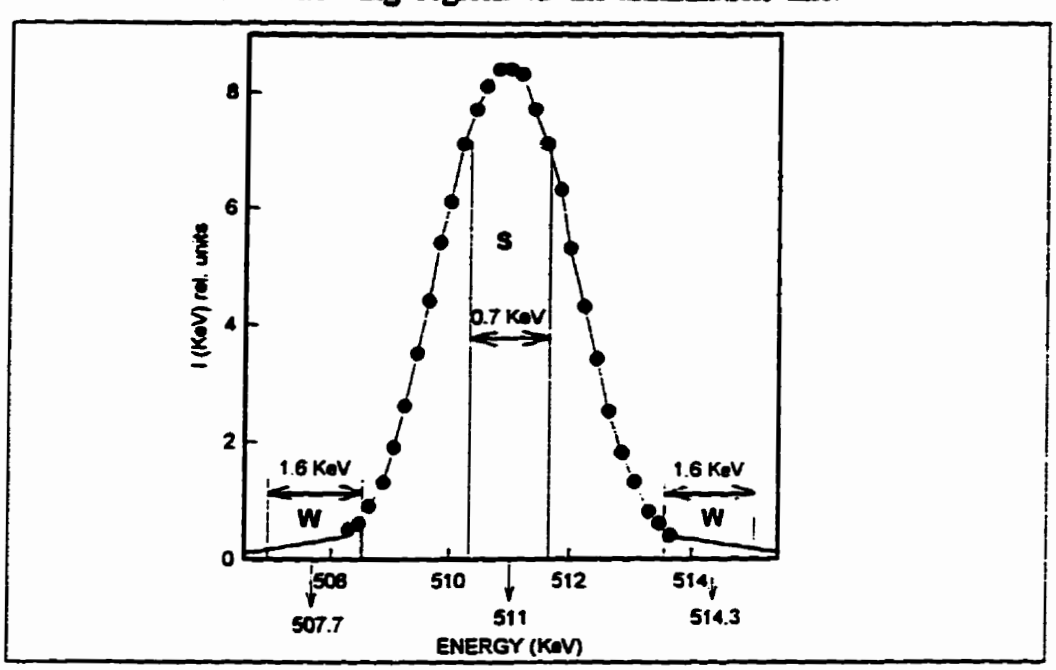

Figure 2.6 Typical Doppler broadening spectra, showing the S and W parameters.

Due to the low momentum of valence electrons, the annihilations fall predominantly inside the region of the S parameter. On the other hand, core electrons have momentum values high enough to contribute significantly to the W parameter. Therefore, the S and W parameters weight the contributions for valence and core annihilation parameters differently.

The absolute values of the above parameters are meaningless because they depend on the position of the windows so only changes of the parameters are of importance. To facilitate comparisons between experiments, it is convenient to report on relative values such as S_D/S_B and W_D/W_B, where S_B refers to the S parameter for the bulk and S_D to the one for the defects. These relative values are practically independent of the energy windows and of the small variations in the energy resolution of the Ge detectors.

The line shape parameters have values characteristic for each material, reflecting the electron-momentum distribution. When positrons are trapped, the lineshape is characteristic of the trapping defect. In a vacancy-type defect, the density of the valence electrons is reduced, which leads to a narrowing of their momentum distribution which is observed as an increase in S. As well, the localized positron in a vacancy type defect has less overlap with core electrons than a free positron, leading to a further decrease in S. The W parameter behaves roughly opposite to S. If only a fraction of positrons is trapped, then the parameters can be expressed as a superposition:

$$S = (1 - \alpha_D)S_B + \alpha_D S_D \qquad (2.8)$$

and $$W = (1 - \alpha_D)W_B + \alpha_D W_D \qquad (2.9)$$

where $$\alpha_D = \kappa/(\lambda_B + \kappa) \qquad (2.10)$$

The subscript B refers to the bulk state and D to the defect state and α_D is the fraction of

positrons annihilating from the defect and is a function of the trapping rate, κ, and the annihilation rate in the bulk state, λ_B. This will be explained in more detail in the next section. As stated before it is only important to report relative values, and using equations 2.8 and 2.9, the following relations can be found:

$$S_D/S_B = \{(S/S_B) + \alpha_D - 1\}/\alpha_D \qquad (2.11)$$

$$W_D/W_B = \{(W/W_B) + \alpha_D - 1\}/\alpha_D \qquad (2.12)$$

2.5 LIFETIME MEASUREMENTS:

2.5.1 FAST-FAST TIME COINCIDENCE SYSTEM:

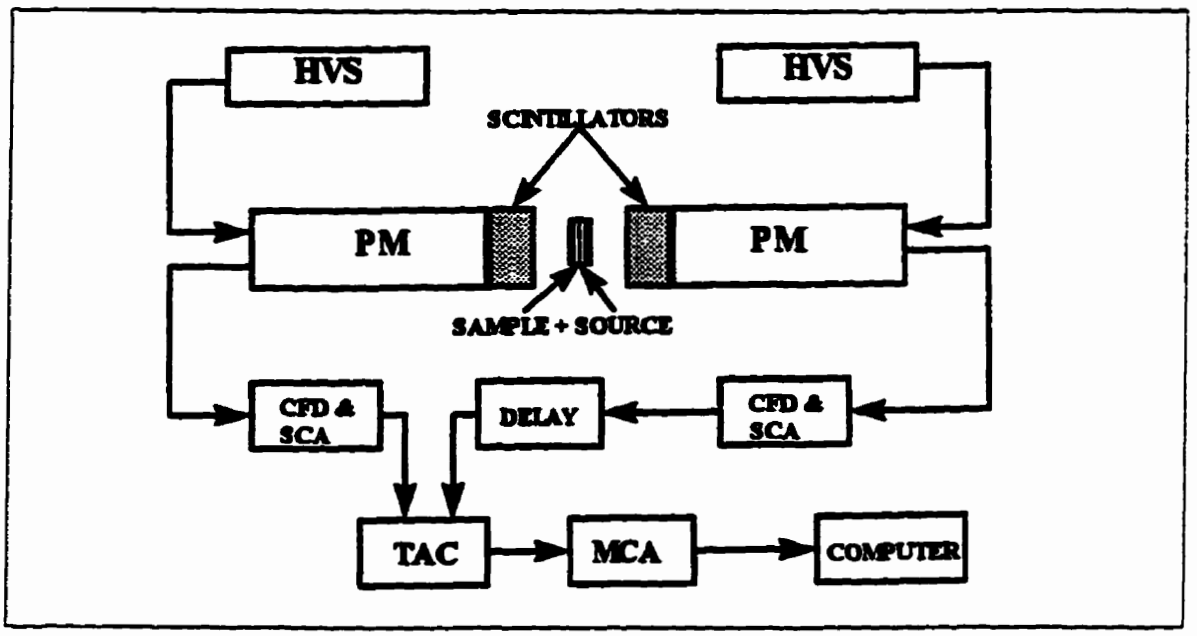

Figure 2.7. Schematic diagram of a typical equipment for measuring positron lifetimes.

Legend:

HVS : High voltage supply.
PM : Photomultipliers.
CFD : Constant fraction discriminators.
SCA : Single channel analyzer.
TAC : Time to amplitude converter.
MCA : Multi-channel analyzer.

In the positron laboratory at the physics department of the University of Winnipeg positron lifetime measurements are performed by means of a fast-fast time coincidence system as shown in figure 2.7. When a positron lifetime spectrum is measured, the situation is the following: simultaneously with the emission of a positron from the source a γ-photon of 1.28 MeV is emitted. The positron is introduced in the sample where it finds an electron and annihilates emitting two photons each of energy 0.511 MeV. The task then is to detect one photon of 1.28 MeV and one of 0.511 MeV and determine the time difference between the two emissions, which then will determine the length of time a *particular* positron lived. The system shown in figure 2.7 does this by means of a start branch connected to detector #1 (1.28 MeV) and the stop branch connected to detector #2 (0.511 MeV).

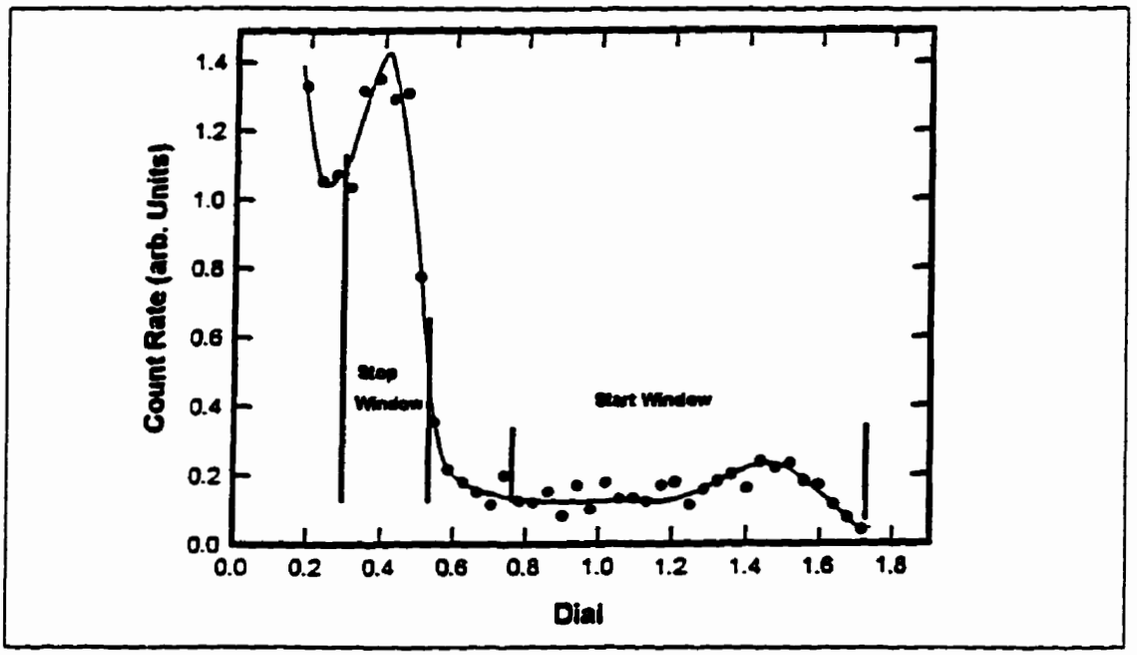

Figure 2.8 Gamma energy spectrum.

The signal from detector #1 is fed into a discriminator circuit (CFD), which gives an output provided the input signal falls within a preselected window of pulses hights from the detector. Choosing detector #1 as the start detector simply means to place the energy window as shown in figure 2.8. The output is then fed into a time-to-amplitude converter (TAC). The stop branch is quite similar to the start branch except that the output from the CFD is first delayed (by ~5 ns) before feeding it into the TAC solely for the purpose of proper operation of the TAC. The output of the TAC is a pulse whose amplitude is proportional to the time difference between the two signals. This amplitude is digitized and stored in a multichannel analyzer (MCA). In this way the channel number in the MCA becomes proportional to the time difference between the two photons (1.28 MeV and 0.51 MeV), and the number stored in each of the channels is the number of events recorded with a certain time difference. Experiments carried out in this laboratory were done using CFD Ortec 583 for both the start and the stop branch.

2.5.2 SCINTILLATOR AND PHOTOMULTIPLIER:

The detection of the gamma quanta is accomplished by a plastic scintillator mounted to a photomultiplier tube [17].

The incident photon enters the scintillator and suffers a large number of interactions which result in exciting the molecules. The excited states rapidly emit visible (or near visible) light; the material is said to fluorescence. The light strikes the photosensitive surface of the

photomultiplier tube, releasing several photoelectrons per photon. These electrons are then multiplied (typically by a factor of 10^5), accelerated, and formed into the output of the photomultiplier tube.

Many different varieties of scintillators and photomultipliers are available, depending on the application in which they will be used. Some of the properties which are usually considered in making the choice includes light output (the fraction of incident energy that appears as light), efficiency (the probability for the radiation to be absorbed), timing and energy resolution. In our case we used Hamamatsu Photonic tubes coupled to a Pilot-U plastic scintillators manufactured by Nuclear Enterprises (decay rate ~0.7 ns) and conically shaped to obtain good timing characteristics. The rather poor energy resolution (see figure 2.8) is a consequence of the fast decay rate, but the fast decay rate is important in obtaining a narrow time resolution of the lifetime spectometer.

2.5.3 POSITRON SOURCE:

The source of positrons used for all the experiments carried out in this work, was the ^{22}Na isotope. The preparation of the positron is done by evaporating a few drops of aqueous solution of $^{22}NaCl$ deposited on a very thin aluminum foil (0.8μm) of size 5x5 mm^2, for encapsulation. The strength of the sources used in the experiments was between 10 to 12 μCi. For the source preparation a new technique was used, which removes the usual ring-like build-up of source material. In this technique the original aqueous $^{22}NaCl$ solution

is first dried out completely in the supplied vial having a conical shaped bottom. Then, using a micro-pipet, five microliters of water is added to form a highly concentrated solution which is then deposited on the source envelope material. Usually two drops (~0.5μliters) are sufficient to produce a 10μCi source which dries forming an evenly distributed layer of ^{22}NaCl with a diameter of about 1 mm. 80% of active material in the vial can be retrieved in this manner. In the experiments done in this laboratory the source was placed between two identical samples of silicon (Si).

2.5.4 THE CONSTANT FRACTION DISCRIMINATOR:

A time pick-off element is essential in all timing systems. An ideal one produces a logic pulse at its output which apparence time-wise is precisely related to the event which caused the pulse. Three sources of error can occur: walk (sometimes called slewing), drift and jitter [18].

Walk is the time movement of the output pulses from the CFD device, relative to its input pulse, due to the variation in the shape and the amplitude of the input pulse. Drift is the long-term timing error introduced by component aging and in particular by temperature variations in the CFD. Jitter is the timing uncertainty of the CFD that is caused by noise in the system and by statistical fluctuations of the signal from the detector.

The following techniques are the most commonly used: Leading edge, where the output logic pulse is produced when the input signal crosses a fixed threshold level. The main

disadvantage of this technique is that the time of occurrence of the output is a function of the amplitude and rise time of the amplitude signal. When the leading edge technique is restricted to applications which involve a very narrow amplitude range of signals, excellent timing results can be obtained. Under these conditions timing errors araise due to charge sensitivity and to jitter. To avoid the serious amplitude sensitivity of the timing signals a new circuit was designed, known as the constant fraction discrimination. In the constant-fraction method the input signal to the circuit is delayed and a fraction of the delayed pulse is subtracted from the original pulse. A bipolar pulse is generated and its zero crossing is detected and used to produce an output logic pulse. Both methods are illustrated in figure 2.9.

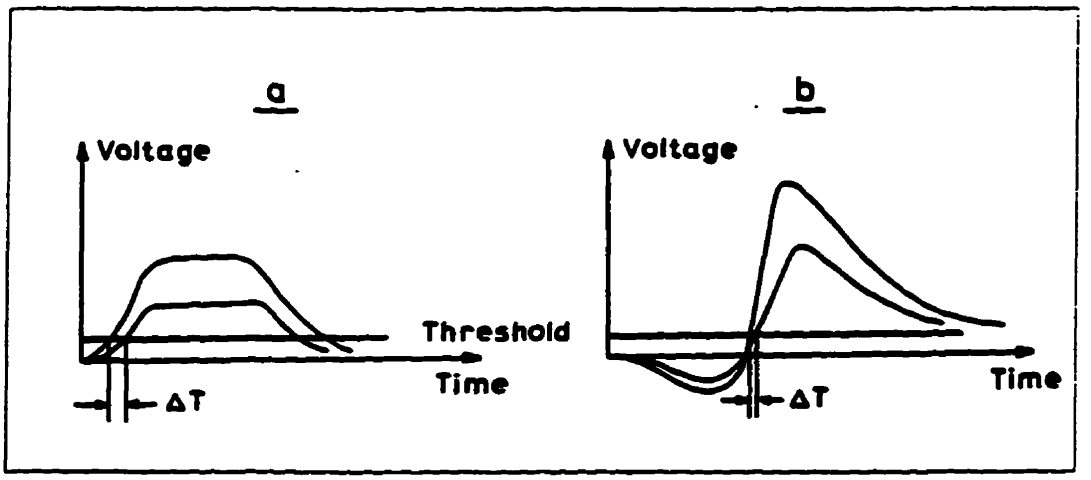

Figure 2.9. Uncertainty in time determination due to different pulse heights by : a) leading edge and b) constant fraction.

As mentioned earlier the CFD generates the timing information and determines also the energy range of interest by means of a single channel analyzer (SCA) build into the CFD unit. If the two detected events fall within the selected energy ranges set by lower level and

upper level controls in the CFD unit, an output is generated.

The proper setting values are extracted from the gamma energy spectrum shown in figure 2.8, defining the start branch as the one that accepts the pulses which arise from the 1.28 MeV γ-quanta and the stop branch which accepts only the 0.511 MeV γ-quanta. Therefore one detector is devoted to the start pulse of 1.28 MeV quanta and the other to the stop of the 0.511 MeV provided they are coincident within the resolving time selected by the time to amplitude converter (TAC) (see below) to within 50 ns of each other.

This ensures nearly completly that a start and stop pulse originate from the *same* positron. However, in a few cases a start and stop pulse can be detected from two different positrons and because these pulses are randomly correlated they give rise to the random background in the lifetime spectra. Background increases with source strength, preventing the use sources of large strength (≥30 μCi).

2.5.5 TIME TO AMPLITUDE CONVERTER (TAC):

The Ortec 556 Time-to-amplitude-converter (TAC) [19] is a module that measures the time interval between a start and a stop pulse and generates an analog output pulse whose amplitude is proportional to the time interval. As explained already above, if the detected events are coincident within the resolving time, the TAC is gated to accept the information. The output of the TAC is fed into the multichanel analyzer (MCA) where a histogram of timing signal differences are accumulated to produce the so called lifetime spectrum as

shown in fig. 2.10.

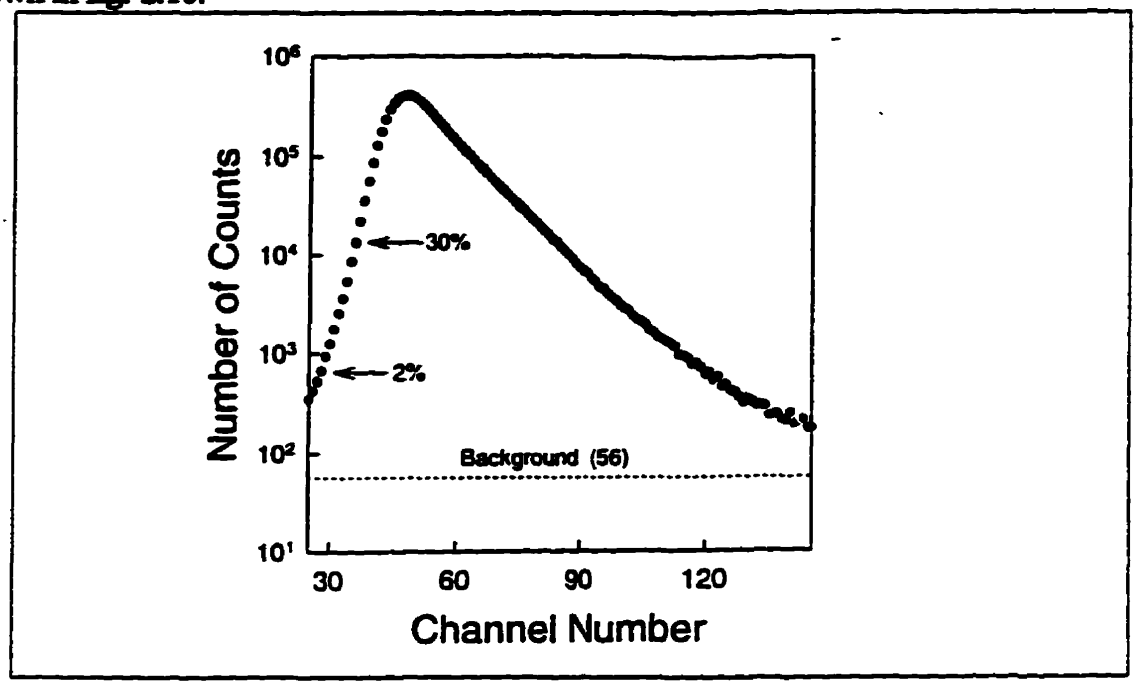

Figure 2.10 Typical positron lifetime spectrum

2.5.6 RESOLUTION FUNCTION;.

Optimization of a lifetime equipment is very complicated and is often a compromise between efficiency and time resolution of the system. The latter is defined as the full-width–at-half-maximum (FWHM), of the so called prompt curve, which is obtained by a source emitting two γ-quanta simultaneously such as ^{60}Co, which emits 1.17 MeV and 1.33 MeV γ-quanta. Such a spectrum is shown in figure 2.11; at normal measuring conditions the FWHM of our equipment is 200 ps. Several theoretical and experimental investigations have been carried out to clarify the different parameters necessary in the quantification of the resolution function. The most important factors are the width of the light pulse generated by the scintillator and, the time spread in the collection of this light on the photo-

cathode of the photomultiplier, as caused by a geometrical size of the scintillator, and finally the transit time spread of pulses traveling from the photocathode to the anode of the photomultiplier. The time spread in the rest of the electronic system is of minor importance when using a good CFD. A continuous development of faster scintillators, their geometrical shapes, photomultiplier-tubes and better discriminators units gradually has reduced the width of the prompt curve. Twenty years ago a FWHM value of 350 ps was considered good, while today its not dificult to obtain 170 ps; and this value is only 30 ps larger than the theoretically minimun resolution value.

In the data analysis the prompt curve is approximated by a sum of Gaussian curves, or, as proposed by W. Puff [12] by summing together gaussians with a single width but with exponentially decaying amplitudes from the centre of the resolution function.

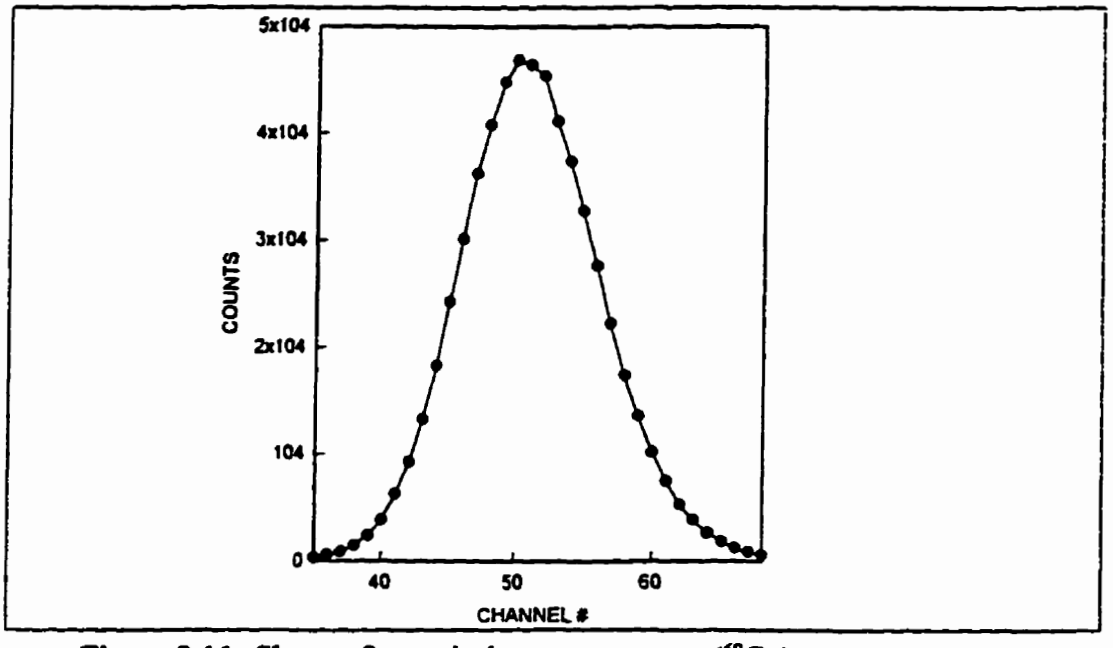

Figure 2.11. Shape of a typical prompt curve, (^{60}Co).

The description of the instrumental resolution curve is an important point, but practical experience shows that the two descriptions mentioned above lead only to small differences in the extracted shape of the curve. Either description is an approximation, and various lifetime equipments can only be expected to behave differently. For this type of reason we have adopted a procedure as described in the next chapter.

2.5.7 CALIBRATION:

The time calibration is basically the determination of the time difference between two adjacent channels in the MCA. This is done by splitting the output signal from one of the CFDs, one is directly conected to the start input of the TAC and the other is attached to a calibrated delay unit, where the output of this unit is connected to the stop input of the TAC. One of the signals is delayed with respect to the other simply by changing the amount of delay in the delay unit. The data is plotted in a delay-time versus channel--number graph, and the slope of the line obtained determines the calibration of the system. The values obtained vary between 24 and 26 ps/channel, depending on the TAC and MCA used for a given system. The uncertainty for a given system is ±0.1 ps.

CHAPTER THREE

ANALYSIS OF THE MEASURED SPECTRA

3.1 INTRODUCTION:

In a measurement of positron lifetimes in condensed material, a spectrum is obtained which generally is assumed to be composed of a number of exponential terms and a background. A widely used computer program by Kirkegaard and Eldrup [21], named POSITRONFIT, was developed to perform a least-squares analysis for extraction of lifetimes and their relative intensities from the experimentally obtained spectra. This program fits a model function to the distribution (spectrum) of experimental data points y_i, which denotes the number of counts recorded in each channel, i, Poisson statistics is assumed to apply. The best model parameters $b_1 \ldots\ldots b_k$ are determined by minimizing the value χ^2 defined by the expression.

$$\chi^2 = \sum_{i=1}^{n} w_i (y_i - f_i(b_i, \ldots . b_k))^2 \quad , \qquad (3.1)$$

where n is the number of data points. Here $f_i(b_i, \ldots b_k)$ is the model value for point number i and w_i the statistical weight attached to this point given by:

$$w_i = 1/\sigma_i^2 , \qquad (3.2)$$

which in the case of the Poisson distribution, equals $(y_i)^{-1}$. For a perfect fit χ^2 will equal one with an uncertainty of one divided by the number of degrees of freedom in the fit. The number of degrees of freedom equal the number of channels incorporated in the fit (511

channels) less the number of fitted parameters (<10).

3.2. POSITRONFIT:

In this program, the model function consists of exponentially decaying components convoluted with the resolution function of the lifetime spectrometer plus a constant background. Let k_o be the number of lifetime components, a_j the decay rate for component number j, R the resolution function and B the background. The model spectrum is given by the following convolution:

$$f(t) = \sum_{j=1}^{k_o} (a_j \otimes R)(t) + B \qquad (3.3)$$

$$a_j(t) = (I_j/\tau_j)\exp(-t/\tau_j) \text{ for } t>0 \quad \text{and} \qquad (3.4)$$

$$a_j(t) = 0 \qquad \text{for } t<0 \qquad (3.5)$$

where I_j is the intensity and τ_j is the lifetime of the j^{th} component. It is assumed that R is given by a sum of k_g Gaussians which may be displaced with respect to each other, according to:

$$R(t) = \sum_{p=1}^{k_g} w_p G_p(t) \qquad \text{where} \qquad (3.6)$$

$$G_p = \{ 1/(2\pi)^{1/2}\sigma_p\}\exp\{-(t - T_o - \Delta t_p)^2/2\sigma_p^2\} \quad \text{and} \qquad (3.7)$$

$$\sum_{p=1}^{k_g} w_p = 1 \qquad (3.8)$$

The gaussian in equation 3.7 is centered around time $T_o+\Delta t_p$ where T_o is a reference time called time-zero (corresponding to time position of the ^{60}Co spectrum, see 2.5.6) and Δt_p a displacement. The standard deviation σ_p is related to FWHM by:

$$FWHM = 2(2\ln 2)^{1/2}\sigma_p \qquad (3.9)$$

The curve given by equation 3.3 is a continuous curve, while the spectra is recorded in channels of the MCA. For proper comparation curve (3.3) must therefore be transformed into a histogram by integration over the width of one channel, with:

$$f_i = \int_{t_i}^{t_{i-1}} f(t)dt \qquad (3.10)$$

where t_i is the value of t at common limit of channel number i-1 and i. as a final result we obtain a model for the least-square analysis of the form:

$$f_i = \sum_{j=1}^{k_o} F_{ij} + B \qquad (3.11)$$

where j represent the value for each component and i the channel number as shown in figure 3.1.

The fitting parameters are the lifetimes τ_p their relative intensities I, time-zero T_o, resolution function parameters and background, B; each of these parameters may be fixed to chosen value.

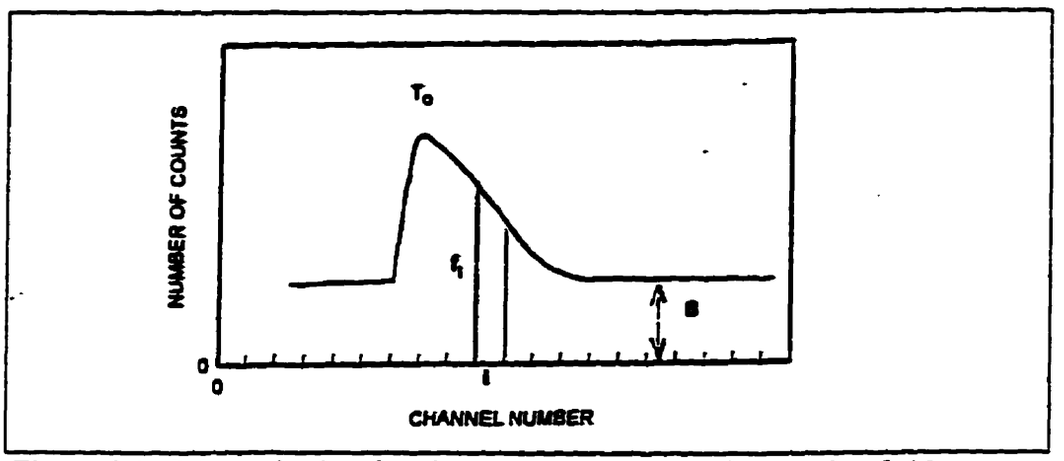

Figure 3.1. Schematic showing the parameters present in equation 3.11.

A least-square technique is applied to fit the spectrum by the mathematical curve given by equation 3.11. POSITRONFIT uses an iterative method called the Marquard's iterative technique. For more detailed information consult references [21-24]. As a final result the following parameters are obtained: lifetimes, relative intensities, background and time--zero-channel and resolution function parameters and all are evaluated with their standard deviations and correlation matrix between the various free parameters. Also the variance of the fit (χ^2) is evaluated. A value of 1.00±0.06 indicates that the chosen model is in perfect statistical agreement with the experimental data.

3.3 EXPERIENCES WITH POSITRONFIT:

In order to resolve lifetime components and their intensities its necessary that the statistical accuracy of the data is adequate. For the work presented in this thesis about $6x10^6$ counts in each spectrum was found to be a good compromise when taking into account the duration of time necessary to accumulate a spectrum. Under favorable circumstances a count rate of 500 counts/sec could be achieved (room temperature measurements) while only

~100 counts/sec were possible for low temperature measurements, due to the large detector separation.

The reader will notice that the number of lifetime components must be supplied by the user of the Positronfit program. To determine that number, χ^2 is a good tool. If too few components are assumed a good fit cannot be obtained. However, this only determines the minimum number of components and does not preclude the existence of further components. By increasing the number of counts it is sometimes possible to resolve further components.

3.4. ANNIHILATION CHARACTERISTICS:

The positron annihilation rate (inverse of positron lifetime) is proportional to the electron density at the site of the positron and is given by:

$$\lambda = \pi r_o^2 c \int dr \, |\psi_+(r)|^2 n(r) \gamma[n(r)] \qquad (3.12)$$

where r_o is the classical radius of the electron, c the velocity of the light, n(r) the electron density and $\gamma(n)$ the enhancement factor of the electron density at the positron site. There are various interpolation formulas for $\gamma(n)$ base on many-body calculations, but all yield values of $\gamma(n)$ which are substantial (≈ 3). Of course, the electron-positron correlations leading to the enhancement are differents in metals, semiconductors and insulators. In the bulk positron state, the positron probes the bulk electron densities, leading to a characteristic lifetime. In a vacancy type defect the electron density is locally reduced and thus the positron lifetime is increased compared to free positrons in the bulk state.

3.5 TRAPPING BY DEFECTS:

As discussed earlier in non-perfect materials, lattice defects can trap positrons. The binding energy to the defect is of the order of 1 eV and arises mainly as the balance between zero point energy of the positron when trapped and the decrease in energy due to smaller overlap of the positron wavefunction with the positive ion cores. Such traps are so deep that thermal escape is neglible so after trapping the positron annihilates in the defect. There are also the so called shallow traps with binding energy of a few tens of meV, (in metal dislocation lines and in semiconductors the Rydberg states around negative ions) from where detrapping may occur. This complicates greatly the experimental situation [25].

3.6.TRAPPING MODELS:

There are two differents model for describing the trapping modes of positrons: The statistical model and trapping model.

3.6.1. THE STATISTICAL MODEL:

The statistical model assumes that an ensemble of positrons during or at the end of the thermalization process have become trapped at various defects or reside in the bulk. In other words, at t=0 (disregarding the slow-down time) the positrons reside in the state from which they annihilate.

3.6.2. THE TRAPPING MODEL:

The trapping model on the other hand assumes that all positrons are in one state at time zero. This state is a delocalized (Bloch) state, and is directly observed in samples which exhibit no trapping of positrons. When defects are present the positrons are assumed to be transferred from the bulk state with a certain rate, κ_i, to the defect. This rate is called the trapping rate, which is assumed to be proportional to the concentration of the i^{th} type of defect according to:

$$\kappa_i = c_i v_+ \sigma \quad \text{or} \qquad (3.13)$$

$$\kappa_i = R c_i \qquad (3.14)$$

Where c_i is the number of defects of type "i" per unit volume, v_+ the thermal velocity of the positrons and σ_i the trapping cross section of the i^{th} defect. R is called the specific trapping rate.

Experimentally obtained lifetime-spectra is, as already explained, analyzed in terms of exponentially decaying terms according to the general form:

$$S_{exp}(t) = \sum_i \lambda_i I_i \exp(-\lambda_i t) \qquad (3.15)$$

Where λ_i is the annihilation rate and I_i the relative intensity. If we denote the probability of the positron to be in a free state as n_B and the probability to be in a defect as n_D, a set of

linear differential equations can be obtained:

$$dn_B/dt = -\lambda_B n_B - \kappa\, n_B \qquad (3.16)$$

$$dn_D/dt = \kappa n_B - \lambda_D n_D \qquad (3.17)$$

The first term of equation 3.16 is the disappearance of positrons from the bulk state by annihilations. The second term is the transfer to trapped states (it is assumed here that detrapping from trapped states into the bulk state does not take place, i.e. they are consider to be deep traps). The second differential equation (3.17) represents the occupation probability for the defect. With the basic assumption that at t=0 all positrons are in the bulk state, the boundary conditions for solving the coupled set of differential equations are:

$$n_B(t=0) = 1 \text{ and } n_i(t=0) = 0 \qquad (3.18)$$

By solving these equations we obtain the total occupation probability, n(t), of the positrons according to:

$$n(t) = \{1 - \kappa/(\lambda_B - \lambda_D + \kappa)\}\exp[-(\lambda_B + \kappa)t] +$$

$$\{\kappa/(\lambda_B - \lambda_D + \kappa)\}\exp[-\lambda_D t] \qquad (3.19)$$

The basic assumption in the trapping model is that at time t=0 *all* positrons occupy the bulk state. From the bulk state the positrons can be transferred at a rate κ (the trapping rate) to a vacancy. Thus positrons will disappear from the bulk by both annihilations as well as transfer to vacancies.

Differentiating n(t) gives the rate by which the positrons disappear, and since they disappear by annihilation only, dn(t)/dt equals $S_{exp}(t)$ from equation 3.15. Thus we find by comparing terms that:

$$I_1 = 1 - I_2 \tag{3.20}$$

$$I_1 = 1 - \kappa/(\lambda_B - \lambda_D + \kappa) \tag{3.21}$$

$$I_2 = \kappa/(\lambda_B - \lambda_D + \kappa) \tag{3.22}$$

$$\lambda_1 \equiv 1/\tau_1 = \lambda_B + \kappa \tag{3.23}$$

$$\lambda_2 \equiv 1/\tau_2 = \lambda_D \tag{3.24}$$

It is inherent to the trapping model that $\lambda_B = \sum I_i \lambda_i$ (with i ranging from i=1 to n) regardless of the number of components, which follows from the assumption that all positrons ocupy the bulk state at t=0. The model can be expanded to involve, for example, two types of defects, D1 and D2 in which case we obtain:

$$I_1 = 1 - I_2 - I_3 \tag{3.25}$$

$$I_2 = \kappa_1/(\lambda_B - \lambda_{D1} + \kappa_1 + \kappa_2) \tag{3.26}$$

$$I_3 = \kappa_2/(\lambda_B - \lambda_{D2} + \kappa_1 + \kappa_2) \tag{3.27}$$

$$\lambda_B = I_1\lambda_1 + I_2\lambda_2 + I_3\lambda_3 \tag{3.28}$$

$$\lambda_1 = \lambda_B + \kappa_1 + \kappa_2 \tag{3.29}$$

$$\lambda_2 = \lambda_{D1} \tag{3.30}$$

$$\lambda_3 = \lambda_{D2} \tag{3.31}$$

Where κ_1 and κ_2 are the trapping rates for defects 1 and 2.

CHAPTER FOUR

BASIC CONCEPTS OF DEFECTS AND SEMICONDUCTORS

4.1. INTRODUCTION:

In this chapter we will introduce the main concepts of defects in crystals caused mainly by high energy radiation which produces defect complexes in a semiconductor. The nature of the radiation damage process involves the creation of Frenkel defects (vacancy-interstitial pairs) caused by collision of incident particles such as electrons, neutrons, protons etc, with atoms and by collisions of the recoil primary atom with other atoms in the lattice. A very considerable amount of work on radiation damage in semiconductors has been reported, in part because the electrical and optical properties of the semiconductors are known to be sensitive to crystal lattice defects. Most of the work on radiation defects in silicon is centered around the positioning of the energy levels in the forbidden band which we will explain in more detailed in this chapter. It is also of interest to study annealing of radiation defects in silicon. These radiation-induced defects have been observed to anneal at a number of different temperatures and we will deal with this theme later in this chapter.

4.2 BASICS OF SEMICONDUCTORS:

4.2.1 INTRODUCTION:

With the development of quantum mechanics, many complex phenomenon in many fields of physics were clarified . One of these fields is solid state physics, which concentrates on the study of solids. But what defines a solid to act as an insulator, conductor or semiconductor?. The answer is given by the band theory of solids.

4.2.2 BAND THEORY:

The atoms in almost every crystalline solid, semiconductor or not, are so close together that their valence electrons constitute a single system of electrons common to the entire crystal.

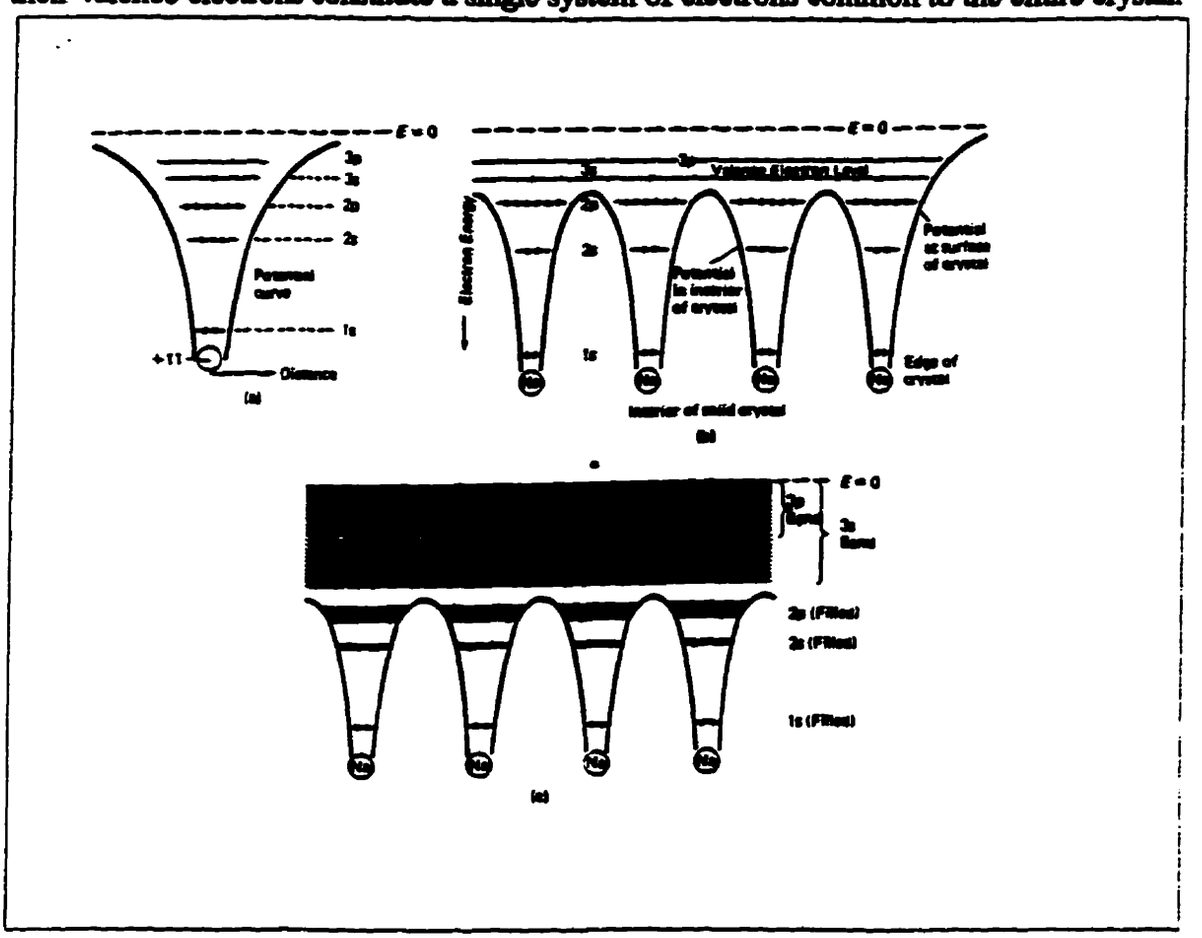

Figure 4.1 Schematic showing the band principle.

a) Energy levels for an isolated Na atom.

b) First approximation of the energy levels of a chain of Na atoms.

c) Energy levels of a chain of Na atoms spread over a range of energy bands.

The exclusion principle is obeyed by such an electron system because the energy state of the outer electron shell of the atom are all altered somewhat by their mutual interactions. In place of a precise energy level of an individual atom, the entire crystal posseses an energy band composed of separate levels very close together. Since there are as many separate lev-

els as there are atoms in the crystal, the band cannot practically be distinguished from a continuous spread of permitted energies.

In figure 4.1 [26] is shown a rough sketch of the energy levels of an isolated atom, which in this example is sodium (Na), There we can see in (a) the occupancy of the different atomic energy levels, and in (b) a chain of one dimensional lattice is formed. In (c) it can be seen that when the atoms are brought together the sharpeness of the energy levels is lost and the result is a continuous set of states known as a BAND. The spaces or gaps between the bands contain no electrons and are called FORBIDDEN BANDS. These gaps constitute the difference in energy between the lowest point of the conduction band and the highest of the valence band.

4.2.3 INTRINSIC SEMICONDUCTORS:

Semiconductors and insulators are differentiated on the basis of their energy gaps. In a semiconductor, the energy gap is small enough that a small but measurable number of electrons are able to jump from the filled valence band to the nearly empty conduction band. Those electrons can now gain momentum in an electric field and lead to electrical conductivity. Furthermore, the corresponding holes in the valence band become now available for conduction because electrons deeper in the band can move up into those levels as they gain momentum. Contrasting this with diamond, the gap is too large to provide a "usable" number of charge carriers, so diamond is classified as an insulator even though not being mate-

rially different from a semiconductor such as Si or Ge. The number of charge carriers increases as we move down through group four of the periodic table to silicon. This conductivity is an inherent property of these materials and does not arise from impurities for which reason they are called intrinsic semiconductors.

4.2.4 EXTRINSIC SEMICONDUCTORS:

Certain impurities and imperfections *drastically* affect the electrical properties of a semiconductor. For example the addition of boron (B) to silicon (Si) increases the conductivity of silicon by many orders of magnitude. The deliberate addition of impurities to a semiconductor is called doping.

4.2.4.1 N-TYPE SEMICONDUCTORS:

Impurities alter the semiconducting characteristics of semiconductors by introducing excess electron or holes. Consider for example the addition of phosphorous to silicon. Phosphorous has five valence electrons rather than four as for silicon. As seen in figure 4.2(a) the extra electron is present independently of the electron pairs which serve in the bonds between neighboring atoms. The extra electron cannot reside in the valence band because it is already full, and so will be located near the top of the energy gap. From this position, called the donor level the electron is easily activated into the conduction band, thus leading to n-type conductivity of the semiconductor.

4.2.4.2 P-TYPE SEMICONDUCTORS:

In this case elements of group III of the periodic table such as boron (B), aluminum (Al), gallium (Ga) or indium (In), are incorporated in the silicon. They have only three valence electrons, for which reason electrons are extracted from the valence band, causing formation of holes in the valence band as can be seen in figure 4.2(b) in the case of gallium in silicon. Each gallium atom can accept an electron. The holes remaining in the valence

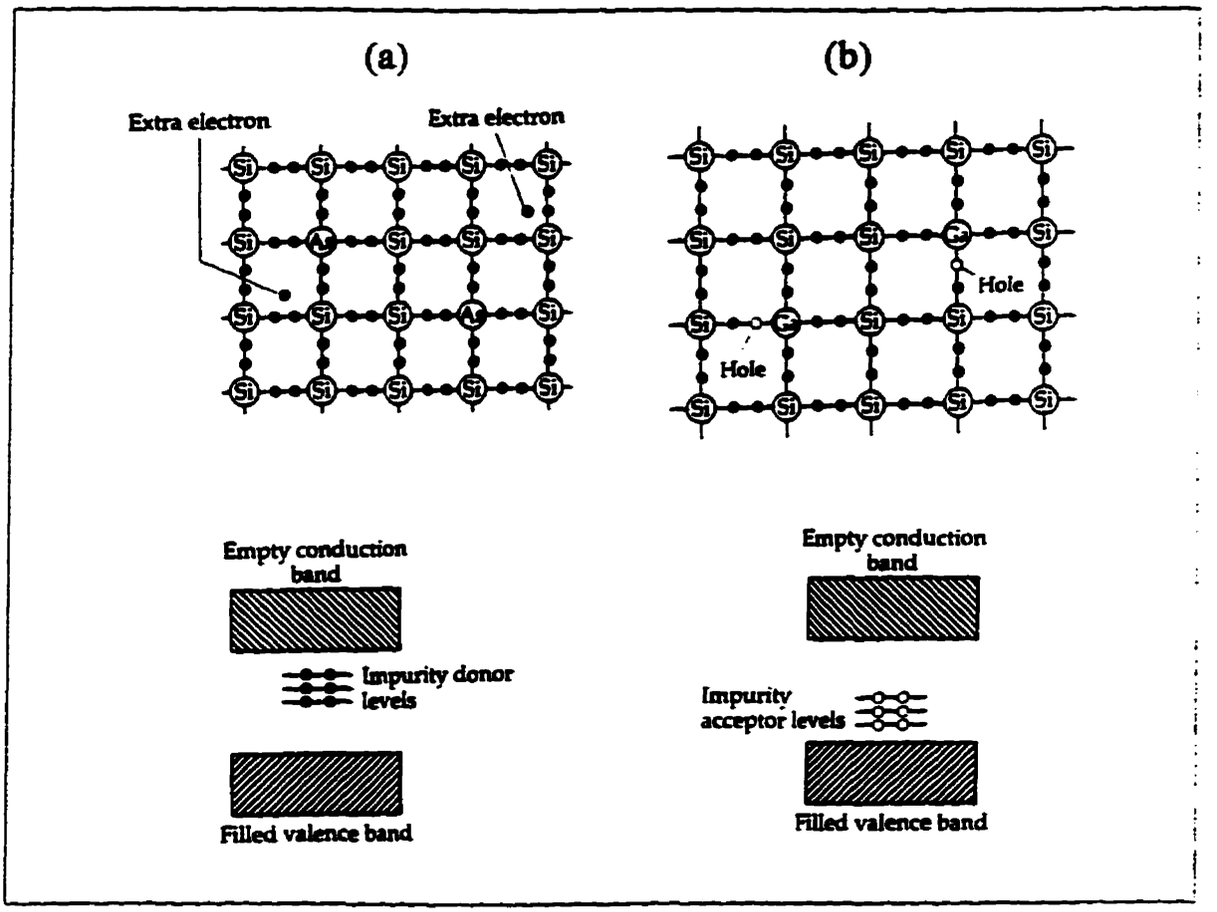

Figure 4.2 Extrinsic semiconductors. (a) n-type impurity and the band model. (b) p-type impurity and the band model.

band are available as positive carriers for p-type conductivity. The electrons in the n-type and the holes in the p-type materials are bound at low temperatures in shallow states. i.e. in

hydrogenic energy levels which are only a few tens of a meV separated from the energy bands. These bound states are diffuse (large orbitals) and contrast with the highly localized states for electron/holes associated with defects giving rise to deep level in the band gap.

4.3. DEFECTS IN MATERIALS:

Defects in crystals arise from deviations of the atoms from their ideal lattice arrangements, and can be classified as follows:

a) Point Defects: Impurity atoms, either inserted into interstitial positions in the crystal or replacing normal atoms. Vacancies constitute the case of the missing atoms and can be monovacancies, divacancies, and larger clusters.

b)Linear Defects: Also known as dislocation lines. They can be characterized by, in one extreme, as an edge dislocation amounting to inserting an extra lattice plane in a part of the crystal. The other extreme is a screw dislocation where an extra plane of atoms is introduced in a stairwell manner. One important aspect of dislocation is that they are potential traps for point defects.

c) Planar Defects: These are imperfections which extend into two dimensions. They can delineate the boundary between different crystallographic direction (twin-boundaries, grain boundaries), but the most severe type is the external surface of the crystal.

4.3.1. POINT DEFECTS:

A point defect is a defect type whose typical size is in the order of atomic sizes. They typically involve:

1)An atom displaced from its regular lattice site (vacancy).

2)An atom located at a different site from a regular lattice structure (interstitial). An interstitial can be of either the same nature as the atoms present in the lattice (self interstitial) or one of a different type.

3) An impurity substituting a normal atom.

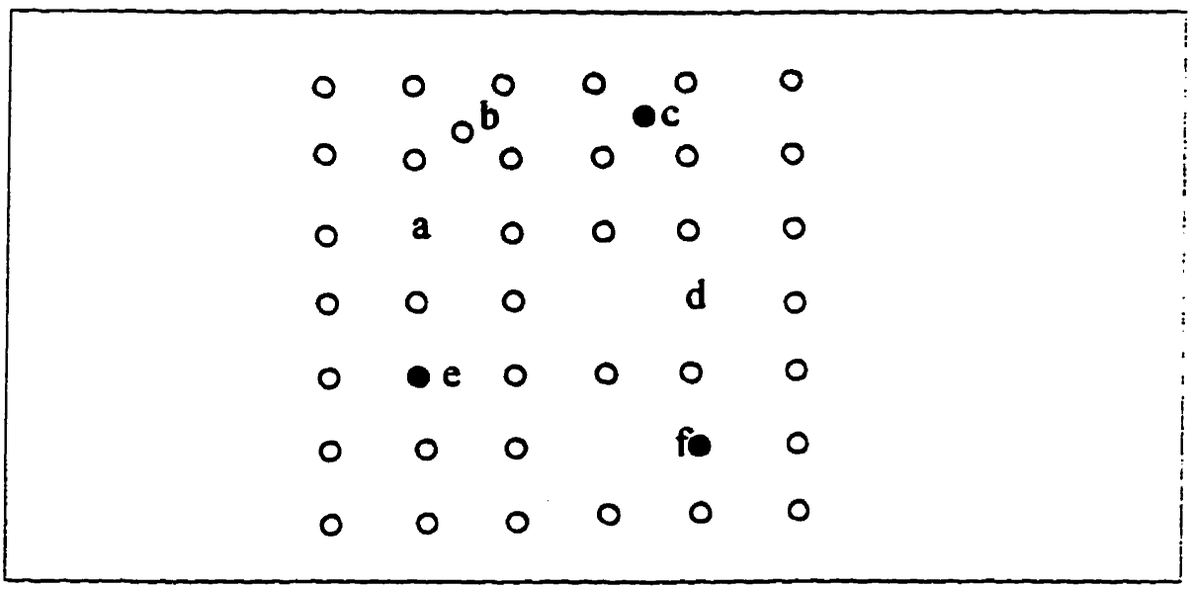

Figure 4.3 Schematic representation of simple point defects: a) Vacancy; b) Self interstitial; c) Interstitial impurity; d) divacancy; e) subtitutional impurity; f) vacancy substitutional impurity complex.

Figure 4.3 [27] shows a simple representation of the point defects, we will explain them in more detail in the coming sections.

4.4. GEOMETRICAL CONFIGURATIONS OF POINT DEFECTS:

4.4.1. THE VACANCY:

When an atom is removed from its regular lattice site a vacancy is created. This creates four dangling bonds which rearrange, and these new bonds can provide localized electrons energy states different from those in the bulk and in some cases these states are situated inside the band gap. Figure 4.4 [27] shows the structure of a vacancy in diamond.

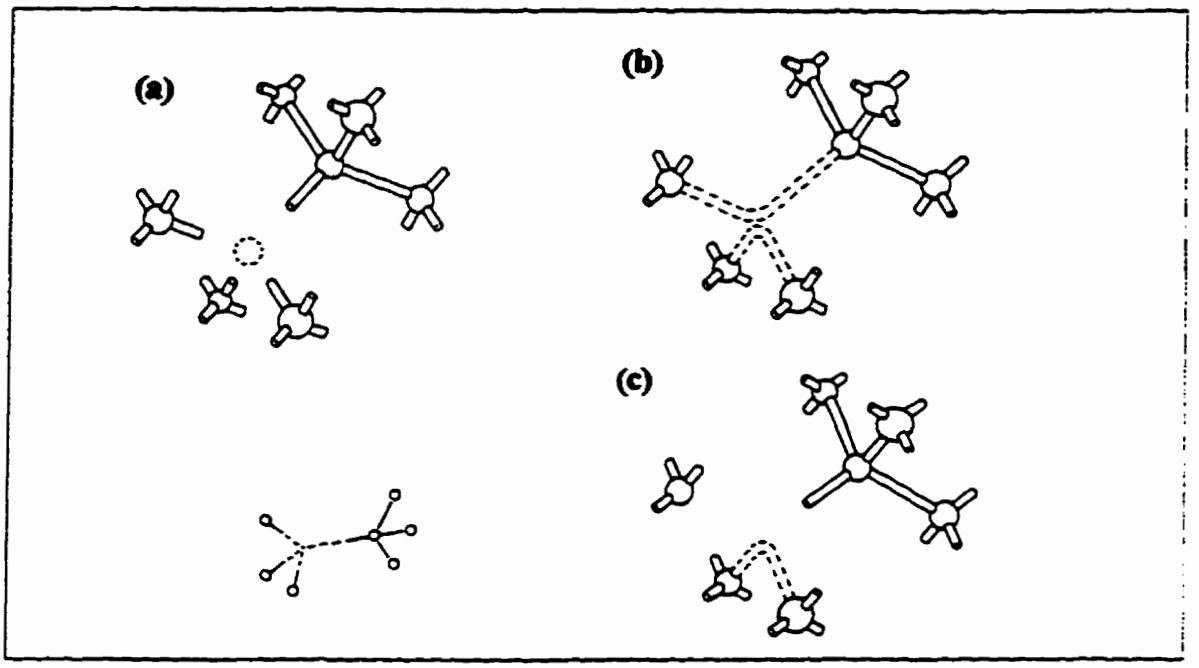

Figure 4.4 The monovacancy in diamond lattice

In (a) the four broken orbitals. (b) rearrangement of the bonds for the case of a vacancy in its neutral charge state (V°). (c) When an electron is missing, in one of these two orbital a positively charged vacancy is formed (V^{+}). The distortion created in the V^{+} is thus different from that of V^{0}. The monovacancy has five charged states ($V^{=}$, V^{-}, V°, V^{+} and V^{++}) inside the band gap.

4.4.2 THE DIVACANCY:

The divacancy is created when two adjacent atoms are removed as shown in figure 4.5. The divacancy is one of the main defects caused either directly by irradiation or the annealing of monovacancies that are mobile at room temperature. The divacancies themselves start to anneal at temperatures of about 150 °C. Also in this case new localized electrons states are formed within the band gap, corresponding to V_2^+, V_2^0, V_2^- and $V_2^=$.

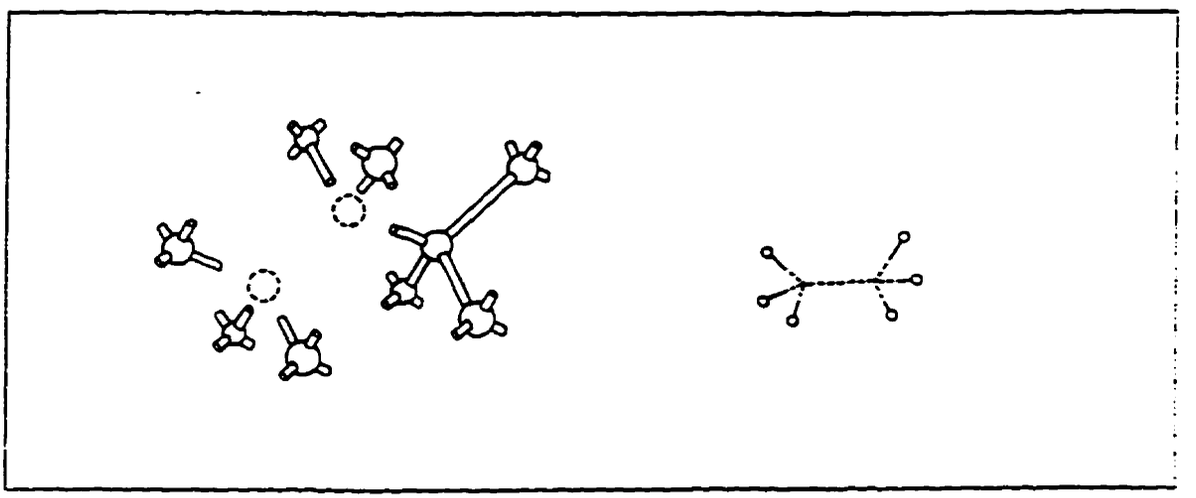

Figure 4.5 The divacancy configuration and its schematic two dimension-representation.

4.4.3 THE INTERSTITIAL:

When an atom is removed from its regular lattice site, this atom is transfered into an interstitial position, and this introduces distortion of the lattice. Its also known that after irradiation damage, many of the monovacancies recombine with the interstitials restoring the lattice to its regular structure. In the case of silicon, interstitials are mobile in p-type material at very low temperatures, while in n-type material they appear to be less mobile, but the ac-

tual mechanism of interstitials migration and the eventual fate of them is still far from understood.

4.4.4 COMPLEX DEFECTS:

Simple defects migrate due to temperature until they are able to reach more stable complex structures. For example, in Cz-Silicon (characteristic for having a large concentration (~30ppm) of oxygen due to its manufacturing process) vacancies start to migrate at temperatures of about 70 K (depending on their charge state), and as a vacancy moves it can be trapped by the oxygen to form VO pairs (vacancy-oxygen pairs), known as the A center. There are other impurities in doped silicon that can trap vacancies such as phosphorous to form VP pairs (vacancy-phosphorous pairs), known as the E center. Also the vacancy can capture another vacancy to form divacancies. For example, in Fz-Silicon (characteristic for having a small concentration of oxygen) the creation of divacancies is the dominant process. Fig 4.6 [27] shows the geometrical configuration of the A center in which oxygen (filled circle) is in a nearly substitutional site.

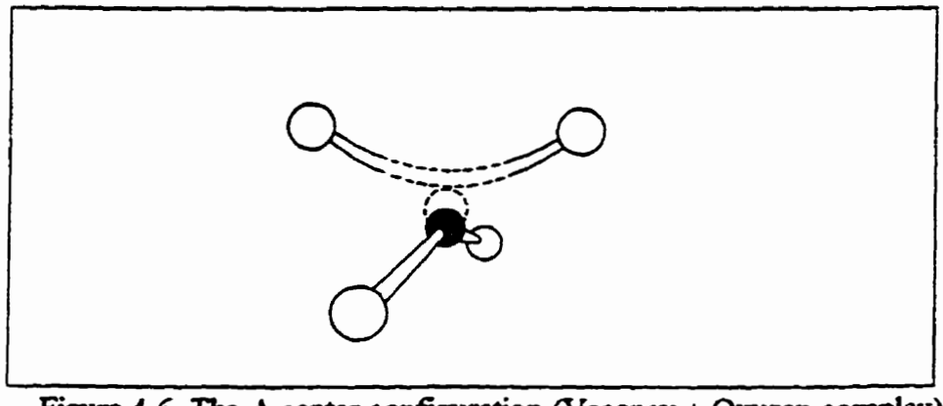

Figure 4.6 The A center configuration (Vacancy + Oxygen complex)

4.4.5 AGGREGATES:

When the temperature increases in a material with high concentration of vacancies these defects form aggregates. As already stated the divacancies start to migrate at temperatures above 150 °C and can form vacancy aggregates such as trivacancies, quadrivacancies, pentavacancies, etc. Little is known about these aggregates because of the large number of possible configurations and also due to their complexity.

4.5 RADIATION EFFECTS IN SEMICONDUCTORS:

The study of damage to solid materials as caused by energetic radiation was prompted by the growth of nuclear technology during the Second World War. In fact a great deal of work on the structure of solids has been done since the discovery of X-rays but these works were concentrated on the structural investigations and little notice was taken of materials which had suffered radiation and gave only slight deviation in the X-ray spectra compared to un-irradiated materials. Since then this field has been ever increasing in importance in the study of many types of materials. Radiation damage represents a way of studying the solids themselves. In particular, radiation provides in many cases a very convenient means of introducing defects in a controlled manner into solids, so that their effects on observed properties can be studied. In the particular case of semiconductors, radiation effects were first observed in 1947 by Lark-Horovitz, Johnson and co-workers [28], in which work they exposed germanium samples to particles such as 10 MeV deuterons and

fast neutrons.

4.5.1. THE INTERACTION OF RADIATION WITH CRYSTALLINE SOLIDS:

Radiation damage in solids has been treated extensively. In the next sections we cover only the basic principles but many excellent review articles, books and conference proceedings are available in the literature[29-31]. The fundamental problem of the interaction of a particle with the crystal is the energy lost by a particle when moving inside matter. In this interaction with the solid, a particle loses its energy by a variety of different processes depending on the type of particle and on its energy. The interaction of the incident particle with the solid can induce the following:

a) Collisions with atoms resulting in excited states.

b) Collisions with electrons of the atomic shells resulting in ionization of atoms.

c) Collisions with conduction electrons resulting in the excitation of an electron gas.

d) Collisions with atomic nuclei resulting in nuclear transformation and nuclear excited states.

The interacting particle can create transient and permanent changes, these are the two basic effects which can be induced in a solid. In the case of transient changes, the effect is non--permanent only as long as the effect of irradiation continues and does not produce any permanent disturbance to the regular crystal structure. In the second case, permanent change means that the displacement of atoms from their normal lattice sites results in a permanent

disturbance of the crystal structure. In this case of crystalline solid bombarded by nuclear particles with sufficiently high energy, enough to break the bond of this atom with the lattice and shift the atom to an interstitial position. This interaction between the nuclear particle and the atom creates a vacancy and interstitial atoms which together form a pair (the Frenkel pair).

The basic damage described above is not a static one and is influenced by the temperature of the solid. As such the defects become mobile, so by increasing the temperature the vacancy-interstitial pairs and impurity atoms start to migrate, producing a variety of different processes of recombination, trapping, replacement, association and disassociation. Let us consider the combination of the processes that can be induced using the three types of point defects generally found in a solid: vacancies (V), interstitial atoms (I) and impurity atoms (D). According to Corbett [32] we shall assume that the energy needed by an interstitial to migrate is much less than that of a vacancy. Then a number of transformations may occur induced by an interstitial.

a) Simple transformations by an interstitial:

1) Recombination between an interstitial and its associated vacancy to form a perfect lattice site. : $I + V = 0$

2) Trapping by a sink(s) such as a surface or dislocations : $I + s = 0$

3) Interaction with other interstitials to form aggregates : $I + I \ldots + I = nI$

4) Replacement with a substitutional impurity atom : $I + D_s = D_i$

5) Trapping by a substitutional impurity atom : $I + D_s = (ID_s)$

6) Trapping by an interstitial impurity atom : $I + D_i = (ID_i)$

b) A vacancy at higher temperatures may induce the following transformations.

7) Trapping by a sink :$V + s = 0$

8) Interaction with other vacancies to form aggregates : $V_1 + V_2 .. + V_n = nV$

9) Interaction with aggregates of interstitials : $V + nI = (n-1)I$

10) Interaction with an interstitial impurity atom : $V + D_i = D_s$

11) Interaction with a substitutional impurity atom : $V + D_s = (VD_s)$

12) Interaction with a complex (ID_s) : $V + (ID_s) = D_s$

13) Interaction with a complex (ID_i) : $V + (ID_i) = D_i$

Thus, having only three types of point defects in the lattice we can expect to observe a large number of transformations processes taking part during thermal annealing.

4.5.2 BASICS OF ANNEALING:

The change of the properties of a defect under the influence of heat, is usually called annealing. An important feature of annealing studies consists of establishing information about the kinetics of defect removal. A commonly encountered situation is migration of defects. Suppose we have an initial concentration of vacancies C_v, then the defect concen-

tration would show a time-change due to migration of vacancies at temperature T according to:

$$dC_v/dt = -AC_v\exp(-E_M/kT) \qquad (4.1)$$

Where A is a constant and E_M is the migration energy.

4.5.2.1 ISOTHERMAL ANNEALING:

Here the time dependence of the defect concentration for constant temperature (T) is studied. The sample is maintained at a fixed temperature for a certain duration of time after which the sample is cooled down to a reference temperature, at which no changes with time take place. The measurement then reveals the change in defect concentration upon the preceding annealing step. Then the sample is again heated to the annealing temperature T, and the process is repeated. The annealing is continued until no changes are observed, i.e. until a steady state is reached. This type of measurement gives a quantitative measure for the activation energy associated with the annealing.

4.5.2.2 ISOCHRONAL ANNEALING:

Here the sample is subjected to a series of annealings where the temperature is raised stepwise, but each step lasts for a certain time interval (measurements are being made for each isothermal step at a low reference temperature). This procedure identifies the temperature at which annealing occurs and identify thus the temperature for isothermal annealing.

4.5.3 IDENTIFICATION OF THE DEFECTS:

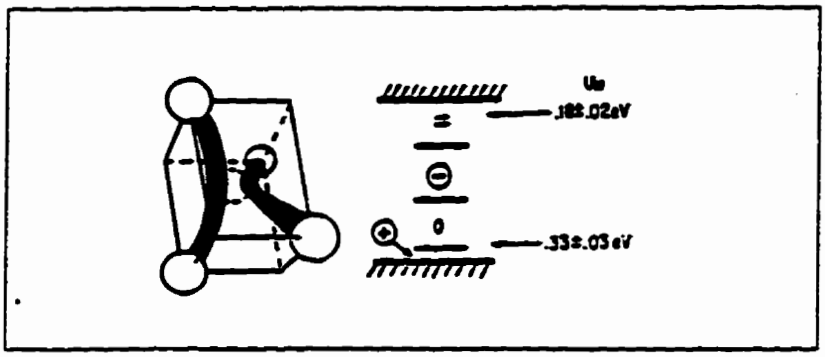

Figure 4.7 Isolated vacancy in silicon as deduced from EPR studies

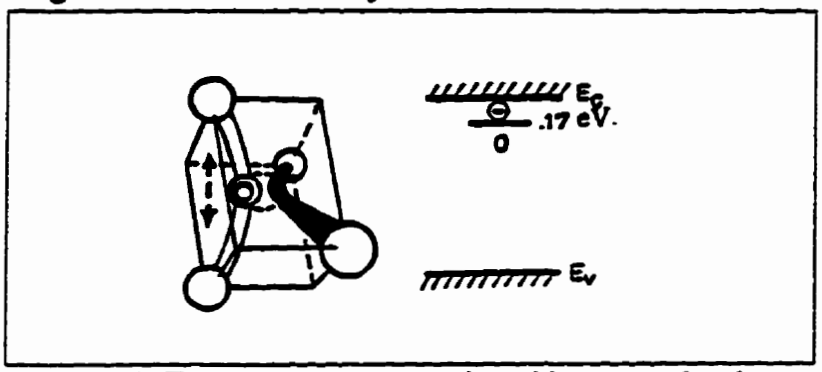

Figure 4.8 The vacancy-oxygen pair and its energy level

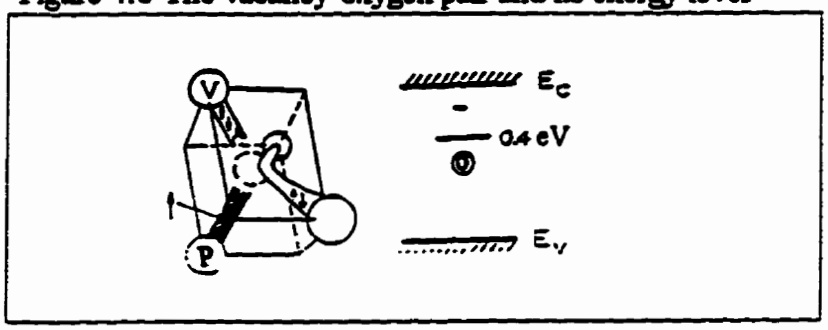

Figure 4.9 Vacancy-Phosphorus pair and its energy level

One of the main objectives of radiation damage studies is defect identification. The defects main characteristics include a structural model, annealing temperatures, migration energies and electronic energy levels.

A great amount of information has been obtained for silicon by the use of several research techniques, being electron paramagnetic resonance (EPR) one of the most important in the

field of defect studies. The isolated vacancy has been observed by Watkins [33] using EPR both in the single positive (V^+) and negative (V^-) charge states. From the dependence of the intensity of the spectra on the position of the Fermi level, the electrical level structure shown in figure 4.7 [29] is deduced. The vacancy has four charge states (V^+, V°, V^-, $V^=$) in the band gap. For the even charge states (V° and $V^=$), the defect is diamagnetic (S=0) and not observed in EPR. The energy levels for even charge states have also been determined using EPR, giving values of 0.18±0.02 eV below the conduction band for $V^=$ and 0.33±0.03 eV above the valence band for V° as shown in figure 4.7. The vacancy-oxygen pair and corresponding electronic energy levels are shown in figure 4.8. and ocurrs as a main defect in Cz-silicon. The vacancy-phosphorus pair (group V impurity) is shown in figure 4.9.

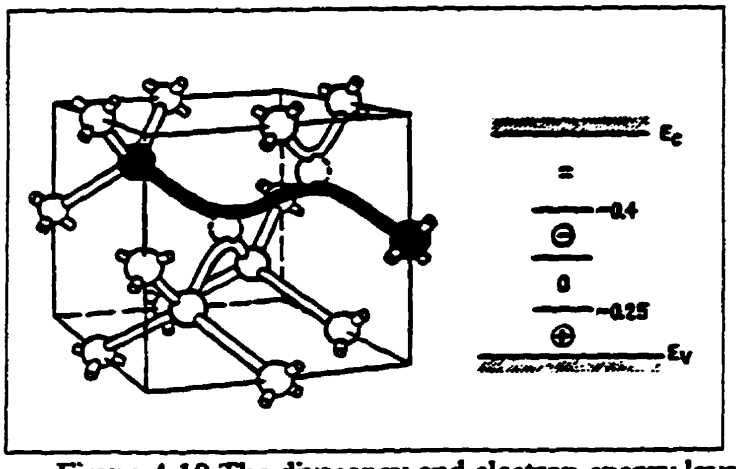

Figure 4.10 The divacancy and electron energy level.

The divacancy and its electronic energy levels are presented in figure 4.10. Finally a summary of electronic energy levels and the deduced (approximate) charge states for various defects in silicon is shown in figure 4.11 [34].

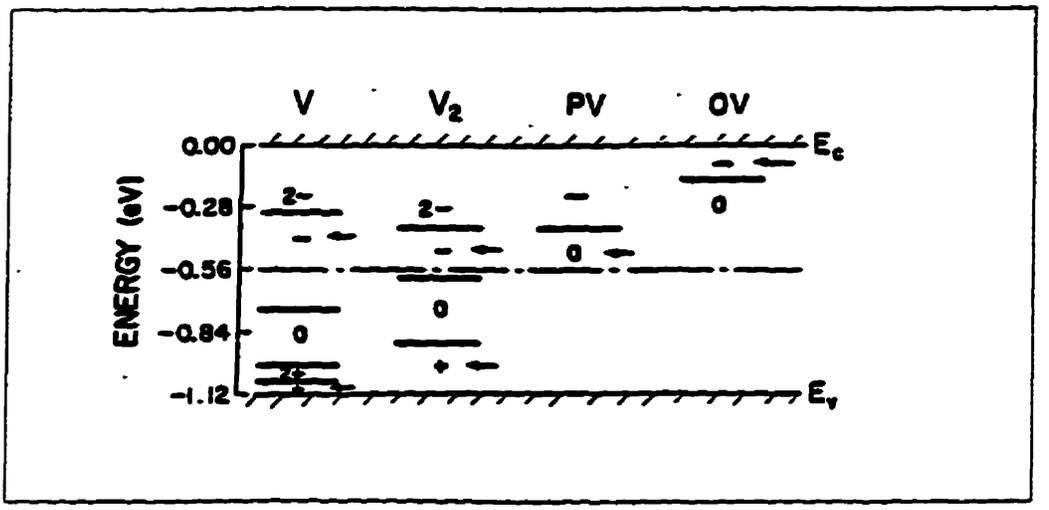

Figure 4.11 Electron energy level positions and deduce charge states defects for various defects in silicon (arrows indicate EPR active charge state).

4.6 OXYGEN IN SILICON:

In this section we will focus on the basics of oxygen-related defects created by electron irradiation and subsequent thermal treatments. The study of oxygen in silicon is a important research field, including electrical, structural and mechanical properties of the crystal and is of large technological importance. A substantial percentage (90%) of silicon crystals used in the semiconductor industry are prepared by the so called Czochralski (Cz) method, pulled from molten silicon in quartz, and contains about 10^{18} oxygen atoms per cm^3 due to the dissolution of silica crucibles (SiO_2).

Isolated oxygen exist in silicon in puckered Si_2O configuration as such oxygen is an electric inactive bonded interstitial. At room temperature oxygen can be detected by finding the 9μm infrared absorption band (stretching mode). Several studies of the strength of this band have produced a correlation with the content of oxygen in silicon materials[35-38].

The 9μm band moves to higher frequencies at low temperatures and splits up into several bands, some of the higher frequency bands are due to a shift in frequency of the Si_2O molecules with different combination of silicon isotopes.

The oxygen solubility in silicon has been found to decrease exponentially with temperature, meaning that at temperatures slightly below the melting point (1450 °C) the oxygen concentration on Cz-silicon is supersaturated and the oxygen precipitates. These precipitates can be electrically active and are therefore a major concern in devices.

A number of experimental measurements on the diffusivity of interstitial oxygen in silicon has given excellent agreement for the diffusion coefficient D in the temperature range of 300-1200 °C and can be expressed by:

$$D=0.17\exp(-2.54/kT) \ (\text{cm}^2/\text{sec})$$

4.6.1 VACANCY-OXYGEN RELATED DEFECTS:

In the following we discuss the defects developing from the vacancy-oxygen (VO) pair (which is essentially a substitutional oxygen atom) to multi-vacancy-oxygen defects during the annealing process. The mechanism by which the VO center is created in Cz silicon exposed to electron irradiation includes interaction between, interstitial oxygen (O_i), vacancies (V) and silicon interstitials (I). The most important reactions are:

$V + I \rightarrow$ annihilation

$V + O_i \rightarrow VO$ (vacancy-oxygen pair)

$VO + I \rightarrow O_i$ (interstitial oxygen)

where vacancies and silicon interstitials are highly mobile at room temperature. The production rate of VO as a function of O_i has shown roughly a linear dependence, as we would expect.

4.6.1.1. THE VO CENTER:

The vacancy-oxygen (VO) center has long been known to be one of the most important defects produced by high energy electron radiation [39,40]. It exists in both a neutral (VO^0) and negative (VO^-) charge state and gives rise to an acceptor level in the band gap at about 0.18 eV below the conduction band. Localized vibrations of the center show infrared (IR) absortion bands at 830 and 877 cm^{-1} at room temperature and 835 and 885 cm^{-1} at low temperatures (≤70 K), for the VO^0 and VO^- states respectively. The VO^- center only exists in materials with the Fermi level above its acceptor energy level. The oxygen atom in the VO configuration is near the substitutional position and bonds to two silicon atoms, as shown in figure 4.6 (p.47).

4.6.1.2 ANNEALING OF THE VO CENTER:

The 830 cm^{-1} absortion band anneals at about 300 °C. This process can be divided into two stages: one fast and the other one slow.

a) The fast process is carbon related (another common impurity in Si at a level of ~1 ppm) and may account for more than 50% of the loss of VO in samples.

b) The slow process normally dominates in cases of low carbon impurity concentration and a new band at 889 cm^{-1} at room temperature appears. The VO complex is assumed to migrate as a whole unit until it is trapped by an interstitial oxygen atom, to form a VO_2 complex.

CHAPTER FIVE

POSITRON ANNIHILATION

AND SILICON

5.1 INTRODUCTION:

In previous chapters we have presented the established models for different defects in semiconductors. Most of the research done on defects in semiconductors has traditionally been Electron Paramagnetic Resonance (EPR) and also by other methods such as Infrared spectroscopy (IR), Deep Level Transient Spectroscopy (DLTS), Photoluminescence and Hall effect. The question to ask is why we need to use positron annihilation spectroscopy (PAS), when we have all these other methods that have provided a wealth of information on silicon in particular, although for other semiconductors the information is much more scarce. Despite this arsenal of techniques there is also a place for positron annihilation, because this technique provides information on vacancies. To establish this technique we should, however, first look for overlap with other methods mainly EPR seeking confirmation of interpretation arrived at by means of positron experimental data. Having first established this, positrons can then significantly extend the "allowed" range of sample characteristics such as temperature and doping among some, and using slow positrons, thin films may also be investigated. As such, positron annihilation gained interest only about fifteen years ago. Before then this technique was used to investigate metals. Significant developments have been made both experimentally and theoretically which without doubt are and will be of value for the study of semiconductors.

5.2 LIFETIME RESULTS:

Before trying to analyze the different defects using the positron annihilation technique, it is necessary to establish basic lifetime values as well as possible, the bulk lifetime being of course very important since all other lifetimes are gauged against this lifetime. For silicon the bulk lifetime has been measured several times with a tendency for ever decreasing values. Presently the value is close to 218 ps as established both on Fz-silicon and Cz-silicon at room temperature and increasing slightly at a rate of only $4x10^{-3}$ps/°C in the 20 °C to 1200 °C range [41]. This makes the bulk lifetime practically constant. The more interesting question is if doping affects the bulk lifetime. Early measurements [42,43] were inconclusive and even though recent measurements on very heavily P-doped Cz-Si [41] do show a lowering of about 4 ps. this is not sufficient to conclude that conduction electrons arising from shallow donors are the reason for the slight changes in the bulk lifetime.

Early lifetime measurements in silicon and germanium showed that the mean lifetime changed upon radiation. Most of the lifetime values are based on irradiated samples and using already established annealing temperatures for defects identified by EPR, the association of a lifetime value with a specific defect was made. This type of procedure of course assumes that EPR data signify defects which are also observed by positrons.

The general trend is that the positron lifetime increases with the size of the vacancy aggregate which is expected according to equation 3.12 (p.31). However, as the aggregate

grows the increment in lifetime diminishes and approaches a theoretical value of 500 ps for large aggregates or voids. Dannefaer et al [44] were the first who succeeded in separating the bulk and defect specific lifetimes in neutron bombarded silicon crystals and demostrated also a strange temperature dependent trapping rate due to negatively charged divacancies. These authors concluded that positrons annihilate with a lifetime of 325 ps. at divacancies and attributed a much higher value of 435 ps. to interaction with quadrivacancies. Fush et al [45] combined Doppler broadening experiments on electron irradiated silicon and gave evidence that at low temperatures (20 K) positrons annihilate at monovacancies and divacancies with lifetimes of 266 and 318 ps. respectively. During annealing the 266 ps lifetime disappear at 150 K, which is consistent with the temperature where vacancies are known to migrate. Dannefaer et al [46] measured the same lifetime, 271 ps, in thermal equilibrium at above 1450 K and assigned it to monovacancies. Positron lifetimes have been calculated by Puska et al [47] and they predicted a lifetime for the silicon vacancy between 254-260 ps. Shimotomai et al [48] have reported lifetimes of 318-327 ps. after 2 MeV electron irradiation at 300 K which they also attributed to divacancies. All of these measurements mentioned above provided the first basis for identifying lifetimes with specific defects. Another interesting lifetime was found by Kelly et al [49] who detected a very short lived component of about 60 ps. in Czochralski grown silicon (Cz-Si), i.e. silicon which is "contaminated" with oxygen to a typical concentration

of $10^{18}/cm^3$. Such a short lifetime has not been observed in float zone refined silicon (Fz) where the oxygen concentration is only about $10^{16}/cm^3$ or less, thus indicating that the growth process of silicon itself is of importance in silicon experiments. A summary of most of the known defects and their associated lifetimes and temperature measurements ranges of are shown in table I.

TABLE I

Defects and associated lifetimes.

Defect	τ (ps)	σ (cm^2)	Temperature dependence	Temperatu. Range
V^0	?			
V^-	270±5 [1-3]	$2x10^{-12}$ - $1x10^{-11}$@20K[3]	$T^{-3.1}$	60<T<120 K
V_2^0	320±5	$\approx 10^{-13}$@300K[4]	T^0	30<T<300 K
V_2^-	325±5	$\approx 4x10^{-15}$@300K[4]		
		$\approx 4x10^{-16}$@300K[5]	$\sim T^{-2.5}$	70<T<300 K
V_2^{--}	325±5	$\approx 8x10^{-15}$@300K[4]	$\sim T^{-2.5}$	30<T<300 K
V_2O^0	270±5	$\approx 10^{-15}$@300K[4]	T^0	30<T<300 K
$VO^0(A^0)$	?			
$VO^-(A^-)$	225±5			
$PV^0(E^0)$	268±5			
$PV^-(E^-)$	248-265	$3x10^{-14}$@20K[3]	T^0	20<T<150 K

#1: Ref.[45]. #2: Ref[46]. #3: Ref[50]. #4: Ref[51]. #5: Ref[52]

5.3 TRAPPING:

Research has indicated that the positron trapping cross section may be strongly temperature dependent by virtue of negative defect charges [44]. According to several measurements the positron trapping rate in semiconductors may in some cases strongly depend on

temperature. When the temperature decreases the trapping rate increases rapidly. For example Makinen et al [50] calculated that the trapping rate into vacancies in silicon increases by a factor of 10 when the temperature decreases from 120 to 20 K. On the other hand in the case of heavily P-doped silicon Makinen at al [50] found that trapping is temperature independent as in metals. In the case of the strongly temperature dependent trapping into vacancies in silicon, Makinen at al [50] estimated that the trapping coefficient at low temperatures reaches gigantic values of 10^{17} to 10^{18} s^{-1}. Shimotamai et al [48] observed the negative temperature dependence of positron trapping, using Doppler broadening, for electron irradiated p-type (B-doped) and n-type (undoped) silicon speciments. Positron trapping has been much less studied in semiconductors that in metals where the subject is well documented both theoretically and experimentally. The process of positron trapping in metals is more or less well understood but this knowledge of positron trapping in metals cannot be directly transfered from metals into semiconductors.

5.4 IMPORTANT REMARKS:

a) The above lifetime measurements have probably identified some of the most important lifetimes in silicon. We must, of course, expect much more complex systems, largely due to the fact that defects may have net charge. To ilustrate this, a monovacancy can exist in five different charge states +, ++,0, -, --, so that positrons may miss entirely the presence of monovacancies if they are positively charged, i.e. when the Fermi level is below E_v+0.1 eV.

For Fermi levels above this value we would expect to observe monovacancies in the neutral or negatively charge states, and we would expect that, when in a negative charge state, the positron trapping section would decrease strongly with increasing temperature, something like T^{-n}, n=2 to 3 [53]. It should be emphasized that this temperature dependence also constitutes a very simple check as to the net charge state of any observable defect, not only the monovacancy, which is very valuable information for defect identification. One pitfall in such experiments is that they can be obscured due to the fact that the Fermi level moves with temperature so that the relative population of two charge states may change significantly bringing about a strong deviation from the T^{-n} dependency of the trapping rate. Of course, the very fact that monovacancies can exist in various charge states and that they migrate at low temperatures [54] makes possible strong interactions with common impurities such as shallow donors/acceptors, oxygen and carbon in Cz-Si. Prominent examples are phosphorous-vacancy pairs (E center, stable to at least 150 °C [55]), boron-vacancy pairs (stable only up to 260 K[56]) and oxygen-vacancy pairs, the A-center, stable up to 300 °C [57]. Apart from the vacancy type defect it must also be that acceptor-like defects are positron traps at least at low temperatures i.e. they are shallow traps. As an example let us consider the A-center. Positrons could be trapped around the negatively charge state of the A-center (just like a hole around an acceptor) yielding a lifetime close to the bulk lifetime, thus complicating any type of analysis significantly. At

low temperatures such effects may well be overwhelming leading to complete trapping in shallow states, a situation which resembles carrier freeze-out in semiconductors. The binding energy would be like shallow acceptor levels i.e. less than 20 meV.

b) *If there were no positron traps, only one lifetime apart from source correction and an* always present ~1.3 ns. weak lifetime would be found. This lifetime, τ_1, corresponds to the bulk lifetime, τ_B, whose value, as explained before, is characteristic of the bulk electron density. When vacancies are present they may trap the positrons resulting in a lifetime , τ_2, whose value is larger than τ_B becauses the electron density in the vacancy is less than in the bulk. When trapping occurs, however, the τ_1 lifetime is reduced below the value of τ_B. This decrease is explained within the framework of the trapping model, because positrons disappear from the bulk state both by annihilation as well by being trapped by the vacancies (see 3.6.2 p.34).

CHAPTER SIX

EXPERIMENTAL RESULTS AND DISCUSSIONS

6.1 INTRODUCTION:

In this chapter we present the results of the experiments performed at the Positron laboratory of the Physics Departament of the University of Winnipeg.

As already explained, the positron annhilation technique has been used by various experimental groups to study simple defects in silicon crystals produced by irradiation. These reseachers have tried to identify in addition to positron lifetime in defect free silicon, the lifetime of positrons trapped at vacancy-type defects such as monovacancies, divacancies, quadrivacancies, vacancy-oxygen pairs and vacancy-phosphorus pairs. We can use these specific lifetimes as input parameters in the analysis of complex positron lifetime data where two or more lattice defects are produced by a high fluence of electron irradiation as is our case. Over the last ten years considerable progress has been made in identifying the defects especially in electron irradiated silicon and in modeling the process by which they are formed. The primary effect of electron bombardement at room temperature is the creation of Frenkel pairs i.e. vacancy and Si interstitials. These intrinsic defects being mobile during room temperature irradiation can subsequentely be selectively trapped next to certain impuritites originally present in the crystal, or else aglomerate to form more stable complexes. Defect complexes are divided into two categories: i) defects created by the interaction among intrinsic defects, such as di-interstitials and the divacancy (V_2). However there is experimental evidence that divacancies can be directly created by a

collision cascade when two adjacent atoms are knocked out of the lattice. ii) defects created by interaction between intrinsic defects and an impurity atom, such as the VO complex. In irradiated phosphorus-doped Cz-Si, vacancies combine primarily with substitutional phosphorus to produce PV pairs or with oxygen to produce VO pairs, since in oxygen-rich silicon (Cz) irradiated by high energy electrons, oxygen is a good trap for mobile single vacancies. This center gives rise to an acceptor level of 0.18 eV. below the conduction band and two IR bands at 830 cm^{-1} (VO^{o}) and 877 cm^{-1} (VO^{-}).

In this work we use lifetime and Doppler broadening mesurements to investigate irradiation damage on undoped Fz silicon (oxygen free) and also on Cz silicon doped with phosphorous, boron and antimony at different concentration levels. In the rest of this chapter we present data as follows: first, radiation damage on Fz-Si is analyzed; second, we present an overview on the effects of radiation on a set of bars of Cz-Si, irradiated with high energy electrons along their long axis, where lifetime, Doppler and optical measurements were obtained as a function of location on the bar, and finally the same set of samples were used to study lifetimes and Doppler broadening as a function of temperature between from 25 K to 300 K.

6.2 VACANCY AGGLOMERATION IN ELECTRON-IRRADIATED FZ-SILICON:

(The work presented in this section, 6.2, was also published in reference [74])

6.2.1 INTRODUCTION:

The purpose of this work is two-fold. First we establish the characteristic Doppler broadening line shape parameter S for divacancies in silicon. Secondly, and perhaps more importantly, we wish to correlate the positron response with that of the 1.8μm infrared absorption band which is linked to the presence of divacancies. This turns out to be a complicated matter.

Three estimates have been reported for the divacancy Doppler broadening S-parameter all based on low-energy positron beam investigations. Makinen et al [58] found saturation of the lineshape parameter corresponding to a 3.8% increase relative to the bulk value for an ion dose above 10^{15}Si/cm^2 while Nielsen et al [59] in a similar experiment found a value of 4.6%. The first authors ascribe this increase to divacancies. More recently, Goldberg et al. [60] estimated 3.3% based on a proton irradiation experiment. Although the three sets of data agree fairly well, none of these experiments does, in fact, prove that the response originates from divacancies.

Here we have combined Doppler broadening and lifetime measurements to investigate 10 MeV electron irradiated Fz-Si, creating defects concentrations much less than necessary for saturating the Doppler parameter. Our experimental situation is therefore much

different from those in the low-energy positron experiments.

6.2.2 EXPERIMENTAL :

The samples were float-zone refined silicon, undoped with a resistivity of 2000 Ωcm, and with an interstitial oxygen concentration below the infrared detection limit of a few times $10^{15}/cm^3$. Irradiation was done using a 10 MeV pulse electron beam (3μs pulses and 240 pulses/s and an average current density of 2 $\mu A/cm^2$) to total dose of $1.2x10^{18}$electrons/cm^2 accumulated over a period of 12 hrs. The sample block, of size 10x10x25 mm^3, was irradiated along its long axis and cooled by immersion in running water at 8 °C. Five samples wafers were cut perpendicular to the long axis of the block and then etched in CP4 removing 0.2 mm of material. The experimental details regarding apparatus, resolution function and source preparation are given in Chapter two of this work.

6.2.3 RESULTS:

The values of the S-parameter are shown in figure 6.1 for both the unirradiated and the as-irradiated sample as a function of sample temperature. The unirradiated sample shows a weak temperature dependence (due to thermal expansion) which contrasts with the strong temperature dependence for the irradiated sample.

Experiments using the low-energy positron beam (operated at 30 keV) at the University of Western Ontario, Canada, on the same irradiated samples showed the same temperature dependency. This demonstrates that the response from our conventional positron source is

the same as that obtained from slow (30 keV) positrons, which only probe a ~3μm deep layer as compared to our average 100μm deep layer.

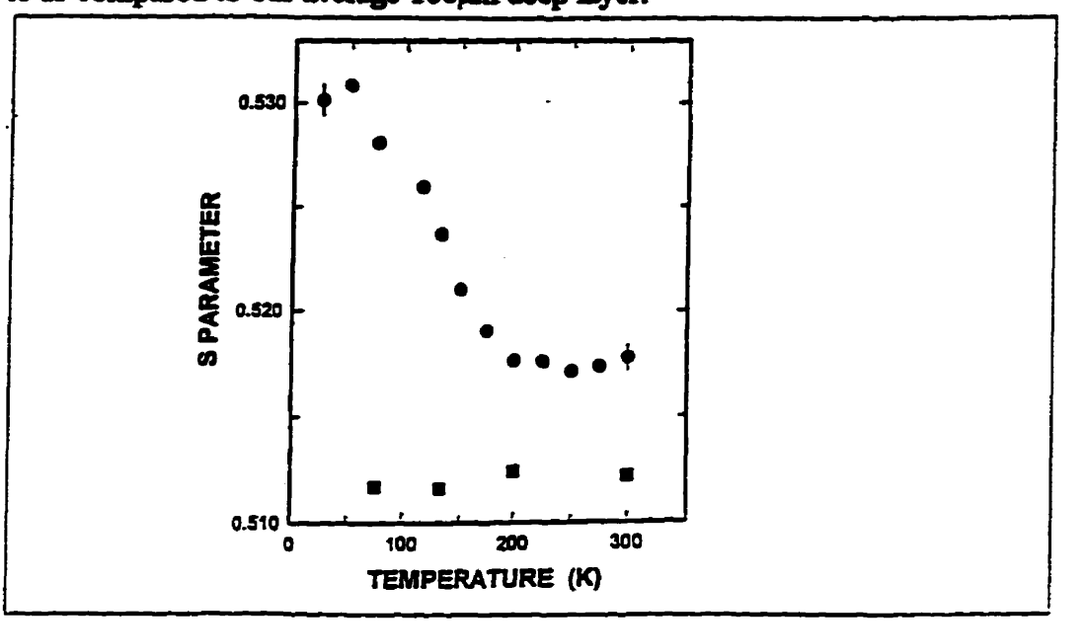

Figure 6.1 Doppler S-parameter for unirradiated (■) an as-irradiated (●) Fz-Si as a function of sample temperature.

The lifetime spectra for the same samples as used in the Doppler experiments could be resolved in two lifetime components in the case of the unirradiated sample. These components had the values of 220 ps and 1.3 ns at 300 K with intensities of 99.9% and 0.1%, respectively The value of the dominating component is close to the bulk lifetime in silicon, albeit slightly larger by 2 ps. [41]. This indicates that some small amount of grown-in vacancies is present but their contribution cannot be resolved. The 1.3 ns lifetime component is rather weak which makes a physical interpretation difficult. It should be mentioned, however, that its value changes systematically from 1.3 ns. at 300 K to 0.65 ns at 30 K. This was found for both the unirradiated as well as for the as-irradiated samples.

For the irradiated sample it was necessary to do three-lifetime decompositions to fit adequately the lifetime spectra. Values of the additional lifetime are shown in figure 6.2, top panel. Its value is close to 305 ps at 300 K decreasing to 290 ps at 30 K and its intensity decreases strongly with increasing temperature as shown in the middle panel.

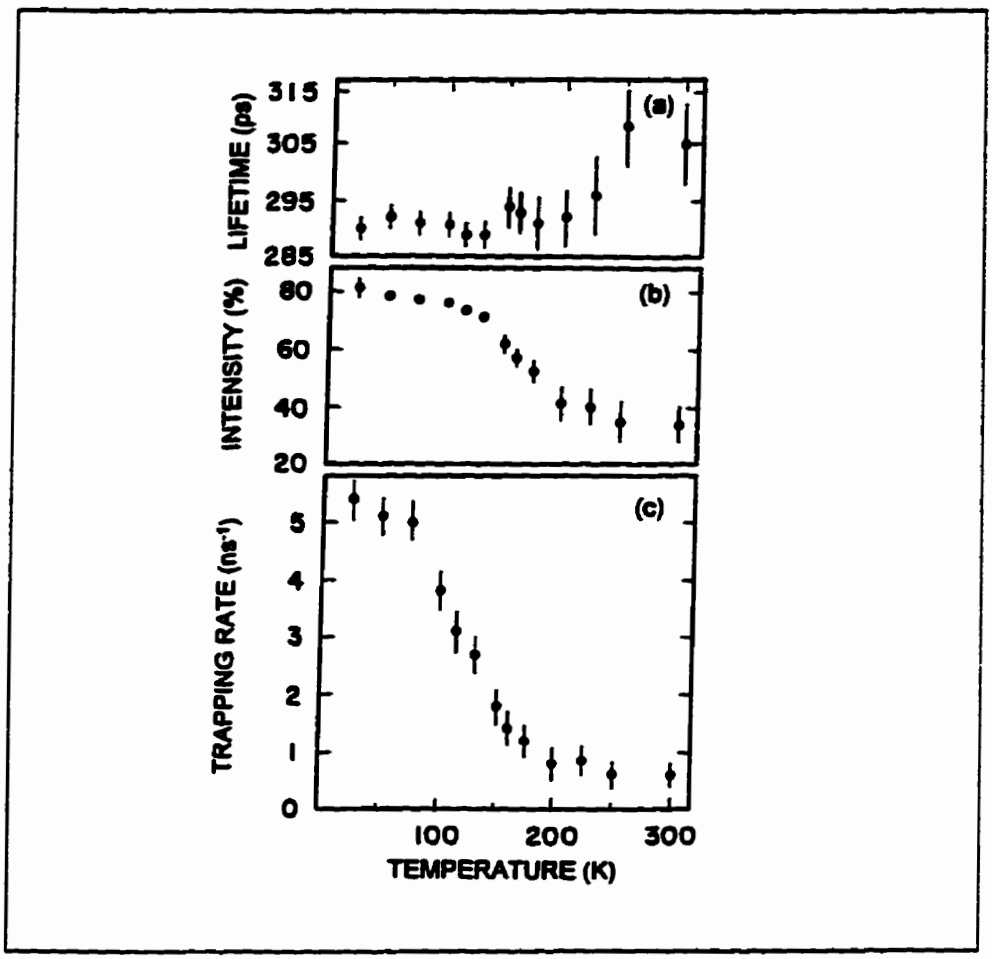

Figure 6.2: Irradiation-produced positron lifetime (a), its intensity (b) and calculated trapping rate (c) as function of sample temperature

The two other lifetime components were the 0.65 ns-1.3 ns component unaltered from the unirradiated case, and a shorter-lived component ranging between 100 and 200 ps.This latter lifetime component was consistent with the simple trapping model [61], (see p33)

thus allowing the calculation of the positron trapping rate for the defects which give rise to the new lifetime component. This trapping rate is shown in the bottom panel of figure 6.2.

TABLE I

Trapped fraction, α, as calculated from the lifetime data and S_D/S_B values for various temperatures of the irradiated sample. Average value of S_D/S_B is 1.067 ± 0.002 when omitting data for the two highest sample temperatures because of the low α values which could be influenced by the pre-existing defects.

Sample Temperature K	Trapped Fraction α	S_D/S_B
25	0.54	1.067
50	0.53	1.072
75	0.52	1.061
115	0.40	1.069
132	0.37	1.063
150	0.28	1.063
175	0.21	1.066
200	0.15	1.073
225	0.16	1.067
250	0.12	1.079
300	0.12	1.088

From the lifetime data one can determine the trapped fraction of positrons α as given by equation 2.10. This allows calculation of S_D/S_B (according to eq. 2.11 p15), the parameter characteristic of the defect responsible for the 305 ps lifetime component. Because the experimentally obtained values of S are arbitrary by virtue of the arbitrary definition of S within the energy spectrum, only changes relative to S_B (the parameter characteristic of the bulk) are of physical importance. All parameters on the right-hand side of equation 2.11 are known in the present work in contrast to the solitary Doppler experiments mentioned earlier [58-60] where α was assumed (quite reasonably) to be 1 for high doses. Table I lists S_D/S_B values which prove essentially constant for large changes in the trapped fraction. This suggests, together with the near-constancy of the defect lifetime, that a single type of defect is responsible for the trapping. This is most likely the divacancy in its singly negative state as will be argued later in the discussion.

The irradiated sample was then isochronally annealed for 25 minutes at each temperature, following which lifetime and Doppler measurements were performed at 50 K. Figure 6.3 shows positron data as well as the integrated absorption of the 1.8μm infrared absorption band (obtained at 300 K). This absorption band arises, according to earlier works, [62-63] from divacancies in any of the charge states +, 0, –, but not from the 2– charge state. Annealing of the positron trapping rate at 50 K deviates substantially from that of the infrared absorption, and the positron lifetime maintains a level close to 290 ps up to 515°C,

well beyond the temperature at which the infrared absorption has disappeared (one further annealing at 600°C was conducted and gave a lifetime of 365 ± 20 ps). The corresponding Doppler broadening parameters S_D/S_B as calculated from equation 2.11 are shown in figure 6.4. S_D/S_B decreases in the same temperature range as did the infrared absorption, attaining a nearly constant level of 1.038 above 300°C. At temperatures above 500°C the calculation of S_D/S_B becomes quite uncertain due to small values of the trapping rate.

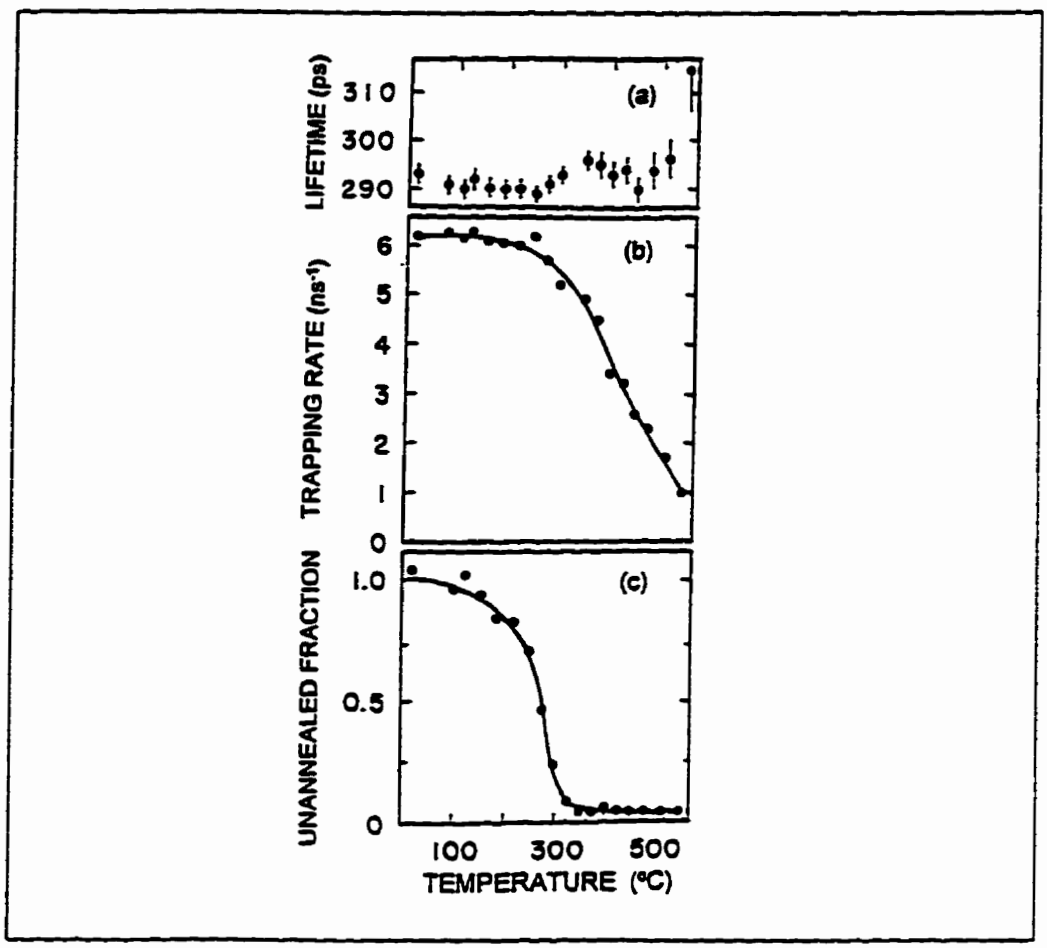

Figure 6.3: Isochronal annealing data of an irradiated sample. In panel (a) is shown the radiation produced positron lifetime and in (b) the trapping rate both for a sample temperature of 50 K. In panel (c) the normalized integrated (between 1.63 and 1.98 μm) infrared absorption is shown as measured at 300 K

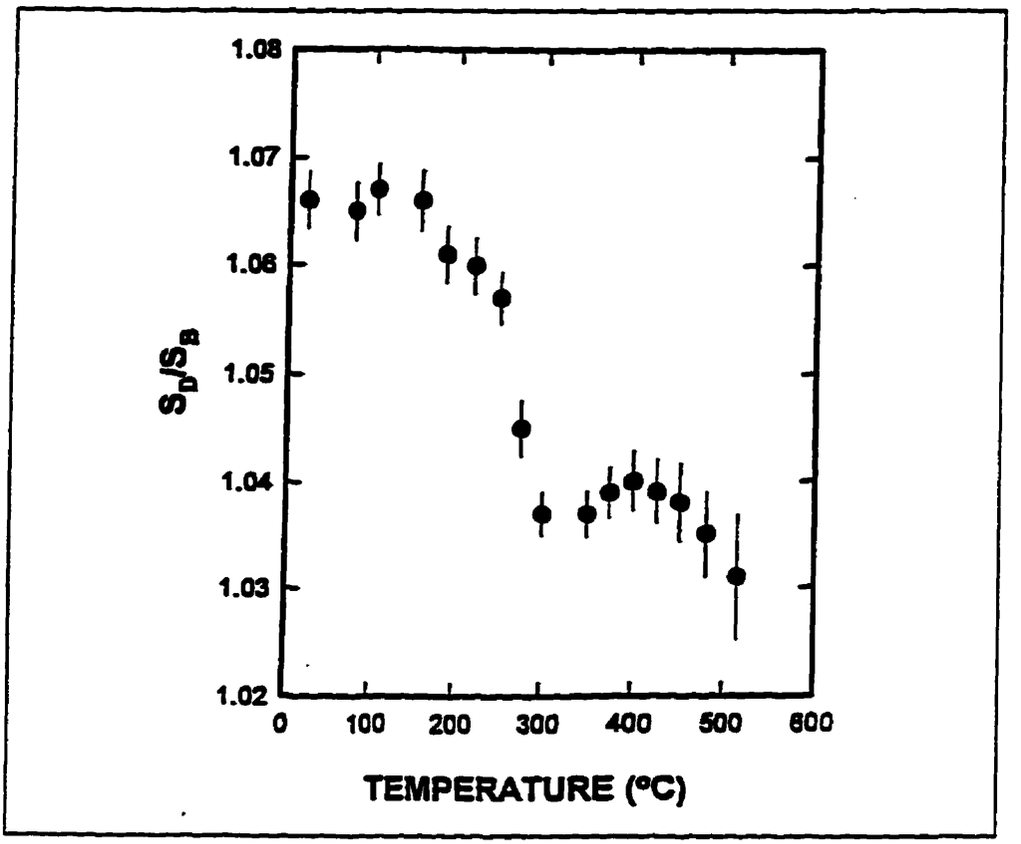

Figure 6.4: Defect specific S_D/S_B as measured at 50 K for the isochronally annealed irradiated sample.

A temperature scan of the samples after annealing at 400°C was done in order to compare with that for the as-irradiated sample. As shown in figure 6.5 the defect lifetime increases much more strongly with temperature than in the as-irradiated case. The trapping rate is still strongly temperature dependent and S_D/S_B shows some (but not a dramatic) temperature dependence. It is clear that annealing indeed has modified the structure of the defects.

6.2.4 DISCUSSION:

The most likely defect type detected by the positrons in the as-irradiated sample is the divacancy. Monovacancies can be ruled out because 1) they are mobile below room

temperature and 2) impurities which could trap monovacancies are too low in concentration to cause detection by the the positrons.

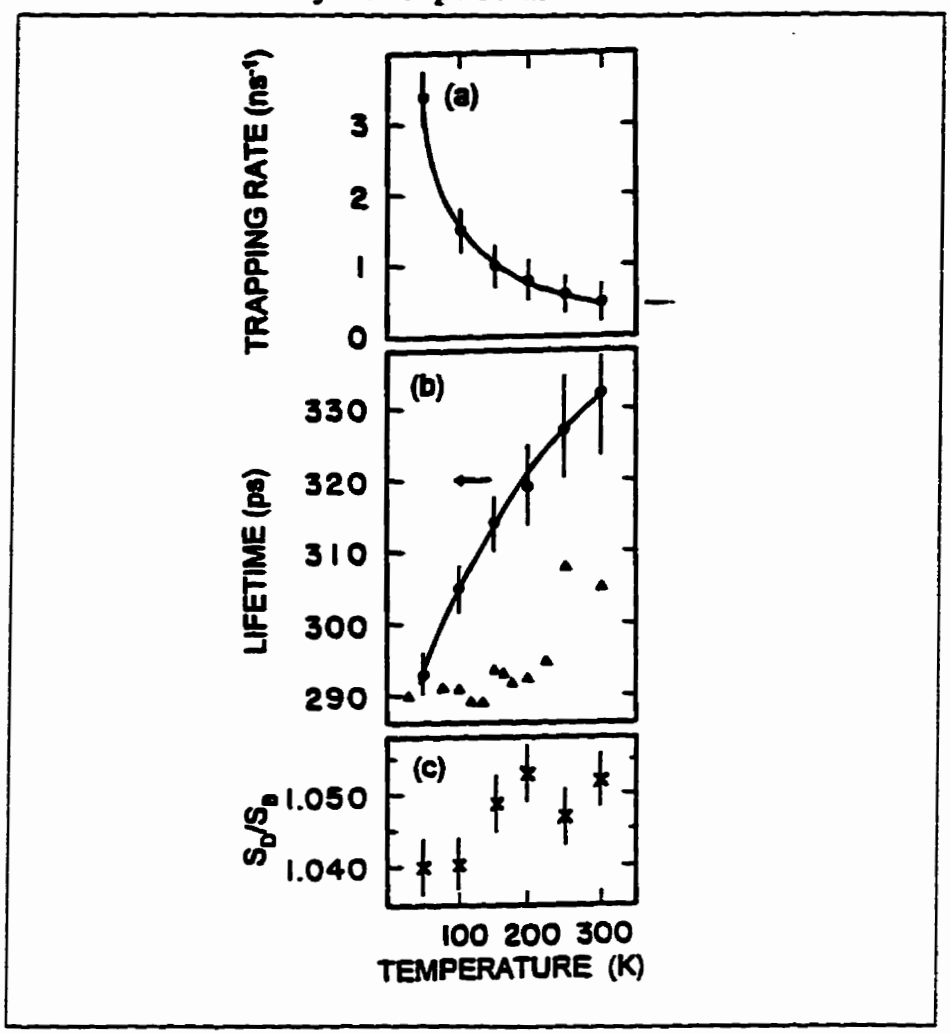

Figure 6.5: Temperature scan of the irradiated sample isochronally annealed to 400°C. In panel (a) the trapping rate is shown. In panel (b) the lifetimes after annealing (●) and before annealing (▲) are shown to facilitate direct comparation. In panel (c) S_D/S_B data are shown for this sample.

The positron lifetime of 305 ps (at 300 K) is indicative of trapping by divacancies, [52,64] and the concentration resulting from the dose of $1.2 \times 10^{18} e^-/cm^2$ agrees qualitatively with that estimated from the introduction rate of divacancies according to Corbett et al. [65] The

current results together with the specific trapping rate for singly negative charge divacancies suggested by Mascher et al [51] yields a concentration of about $1.5x10^{17}/cm^3$ while a more recent estimate of the specific trapping rate by Kawasuso et al. [66] results in a smaller concentration of $0.6x10^{17}/cm^3$. For comparation, the introduction rate of Corbett et al [65] (albeit for positively charge divacancies) suggests a concentration of $0.4x10^{17}/cm^3$. Kawasuso et al. [67] have futhermore found from isothermal annealing of their ≈300 ps lifetime an activation energy of 1.3 eV in good agreement with the divacancy interpretation based on earlier infrared [63] and electron paramagnetic resonance measurements [65].

The next point to consider is the charge state of the divacancies. The strongly temperature dependent trapping rate (Fig. 6.2 and 6.5) is commonly taken as evidence for a negatively charged defect [51,68], but recently Kawasuso et al [64] have suggested a similar behavior for neutral divacancies. From a theoretical point of view it is difficult to understand how a neutral defect can behave as a negatively charged defect because the former lack the attractive long-range coulomb potential. We also point out that Kawasuso et al [64] assessed the charge state of the divacancy using the electronic level deduced from deep-level-transient spectroscopy [69] which places the 0/– level at $E_c - 0.4$ eV, where E_c is the bottom of the conduction band. Had the lower level of $E_c - 0.54$ eV instead been used as deduced by Young and Corelli [70], this would have led to the conclusion of a negative charge. In view of the above reservations we maintained that the strong

temperature dependence of the trapping rate indicates negatively charged divacancies. Since the 2– charged divacancy does not give rise to the 1.8μm absorption band [62] it is most likely that the divacancies observed in this work are singly negative.

In summary, the above discussion strongly suggests that in our samples 10 MeV electron irradiation introduced divacancies. The positron lifetime of 300 ps and the 1.8μm absorption band are the main indicators therefore and, according to Table 6.1, the lineshape parameter is 6.6% larger than that for the bulk. This value is nearly twice the value hitherto estimated from the solitary Doppler experiments [58-60]. A possible explanation for this discrepancy will be offered after discussing the implications of our annealing data.

These data exhibit three unexpected features. 1) By associating the 300 ps lifetime component with divacancies one would expect that the trapping rate should anneal in the same manner as the 1.8μm infrared absorption band, but this is clearly not the case (see fig. 6.3). 2) Upon annealing above 150 °C one would expect vacancy agglomeration arising from migration of divacancies and hence an increase in lifetime. There is no indication for this according to figure 6.3 at least up to an annealing temperature of 515°C. 3) Vacancy agglomeration would be expected to increases the value of S_D/S_B, but a decrease is in fact observed (see Fig. 6.4).

We suggest the following model to explain these observations: Upon annealing above ~

150°C migration of divacancies forms clusters, but they are initially "loose" in the sense that the individual vacancies have not coalesced completely. Only at sufficient high temperature final coalescence takes place to form a continuous multi-vacancy complex. The disappearance of the 1.8μm absorption band we then suggest is a consequence of a significant distortion of the divacancy when becoming part of the loose cluster, perhaps to the degree that in such a cluster vacancies should rather be viewed as an assembly of individual monovacancies. The S_D/S_B data in figure 6.4 lend support to this suggestion because a change from isolated divacancies to a loose cluster of monovacancies would decrease rather than increase S_D/S_B. This interpretation implies that the value of 1.038 for S_D/S_B might be comparable to that for monovacancies. The idea of a loose cluster of monovacancies (a "sponge" defect) was originally proposed by Hornstra [71] and discussed by Corbett and Bourgoin [72] although at the time there was no experimental support for such a structure.

For such a loose vacancy cluster one would expect that sample temperature would be a stronger influence on positron parameters than for a divacancy. This is observed (see Figure 6.5). The positron lifetime and S_D/S_B increase substantially with temperature in contrast to the case of the divacancy. It should be noted that judged from the trend of lifetime with temperature, a lower sample temperature than 50 K would have produced a lifetime less than that for the divacancy which supports the idea of a monovacancy

constituent of the cluster. Whether the change in lifetime is a result of a temperature dependent configuration of the clusters or arises from a change in the localization of the positron within the cluster is not clear although we do hold the latter possibility more likely than the former. Finally, we note that annealing at 550°C results in lifetime of 315 ps at 50 K (at 600°C the lifetime was 365 ps and independent of measurement temperature). This suggests that above ~ 500°C final coalescing of the loose vacancy cluster takes place.

Above has been presented a model which can explain the experimental results, but one item has not been discussed so far, namely the mechanism(s) by which the trapping rate decreases over the very wide temperature range of 150-550°C. We have argued that the disappearance in the 150-300°C range of the infrared absorption band is due to coalescing of vacancies. This could well account for the rather small decrease in the trapping rate of 20%. But when the coalescing has been completed long-range migration of vacancies seems unlikely which then raises the question why the trapping rate continues to decrease. Three possibilities present themselves. The first invokes release of the irradiation-produced interstitials from (unspecified) traps whereupon the overall vacancy concentration would decrease. The second possibility is a gradual change in the charge states of the clusters. The third possibility is that even without a change in the charge state a small binding energy for the positrons could change slightly. This latter possibility presupposes that the clusters are negatively charged, for which there is a definite indication by virtue of the strong

temperature dependent trapping rate shown in fig. 6.5. Any of these possibilities could be invoked to explain the decrease in trapping rate.

In closing this discussion, we return to the discrepancy between the here advocated S_D/S_B value for divacancies of 1.067 and that suggested from the solitary Doppler broadening experiments of 1.033-1.046 [58-60]. This we suggest to arise from experimental conditions, because in the solitary Doppler experiments the defects were created by ion (or proton) irradiation to a concentration at least 100 times that utilized in our work. This could create many vacancy clusters clusters of the type proposed here so that the results from the Doppler experiments should rather be compared with our values obtained after annealing above 300°C in which case we obtain a remarkably good numerical agreement.

6.2.5 CONCLUSION:

This work has reaffirmed the lifetime value of 305 ps at 300 K (290 ps at 30 K) for isolated singly negative divacancies in silicon. The Doppler parameter S_D/S_B was found to have a value of 1.067 ±0.002. Annealing between 150 - 300°C is proposed to create loose multivacancy complexes in which the positron can be localized at low temperatures in the monovacancy part. Upon annealing the 1.8μm infrared absorption vanishes and the value of S_D/S_B decreases to 1.038 ± 0.003. Annealing above ≈ 515°C is necessary for the formation of actual vacancy clusters.

6.3 AN OVERVIEW ON EXPERIMENTS PERFORMED ON CZ-SILICON IRRADIATED WITH HIGH ENERGY ELECTRONS:

6.3.1 INTRODUCTION:

Next we present an overview of the defects created in Cz-Silicon by irradiation with high energy electrons. A set (see table II) of rectangular wafers (30x4x0.5 mm^3) were irradiated along the long axis of the bars. The set consisted of eight pairs of Cz-Si doped with phosphorous, boron and antimony in different concentration levels. In this work we use only lifetime and Doppler broadening techniques. The focus of this work is directed toward examining the types of defects induced in the material, as influenced by the dopant fluence levels and the distribution of defects along the wafers.

6.3.2 EXPERIMENTAL:

The characteristics of the samples used in these experiments are shown in Table II. These wafers typically contain interstitial oxygen at a concentration of about $10^{18}/cm^3$. Two sets of the eight different pairs of Cz-Si were cut from the wafers. One of the sets was left unirradiated for reference measurements. The second set was installed in a specially designed device to hold the eight pairs in the direction along the long axis of the bars relative to the irradiation beam. The bars had a separation of 0.5 mm to allow the 8 °C running water to flow between them as coolant. The irradiation was done using a 10 MeV pulsed electron beam to a fluence of $1.2x10^{18}$ e^-/cm^2 accumulated over a period of 12 hrs.

TABLE II

Samples characteristics

Code	Dopant & Type	Concentration atoms/cm^3	Resistivity Ω-cm
P-4	P(n)	$5x10^{18}$	0.01
P-3	P(n)	$5x10^{17}$	0.1-0.2
P-2	P(n)	$5x10^{16}$	1-2
P-1	P(n)	$2x10^{16}$	3
Sb-4	Sb(n)	$1x10^{18}$	0.01
B-4	B(p)	$5x10^{18}$	0.01
B-3	B(p)	$5x10^{17}$	0.1
B-0	B(p)	$4x10^{14}$	100

The details of equipment and procedure have been presented in Chapter 2 of this work. The unirradiated samples were measured at three different positions along the bars. No difference could be detected for the different positions and an average bulk lifetime of 218±2 ps, was found, which agrees well with that obtained from the Fz-Si just described. The irradiated samples were first investigated by lifetime measurements as a function of location along the bars; these were taken about 5 mm apart starting at the end which received the highest amount of radiation to the other end of the bar (a total of seven positions were measured). Doppler broadening was also done on these bars as a function of position, but in this case only three positions were measured, one at each end plus one at the center. Temperature dependent measurements were done on the irradiated samples but only at the end that received the highest amount on radiation.

6.3.3 RESULTS FOR TEMPERATURE EXPERIMENTS:

6.3.3.1 N-TYPE SAMPLES:

The results for n-type samples are presented in figure 6.6, where the irradiation-produced lifetime is shown in panel (a). The high-concentration phosphorous doped P-4 sample has a constant lifetime of 260 ps between 20 and 300 K and an intensity of 100%, which shows that in this case complete trapping was reached, indicating that positrons were trapped by a high concentration of VP pairs.

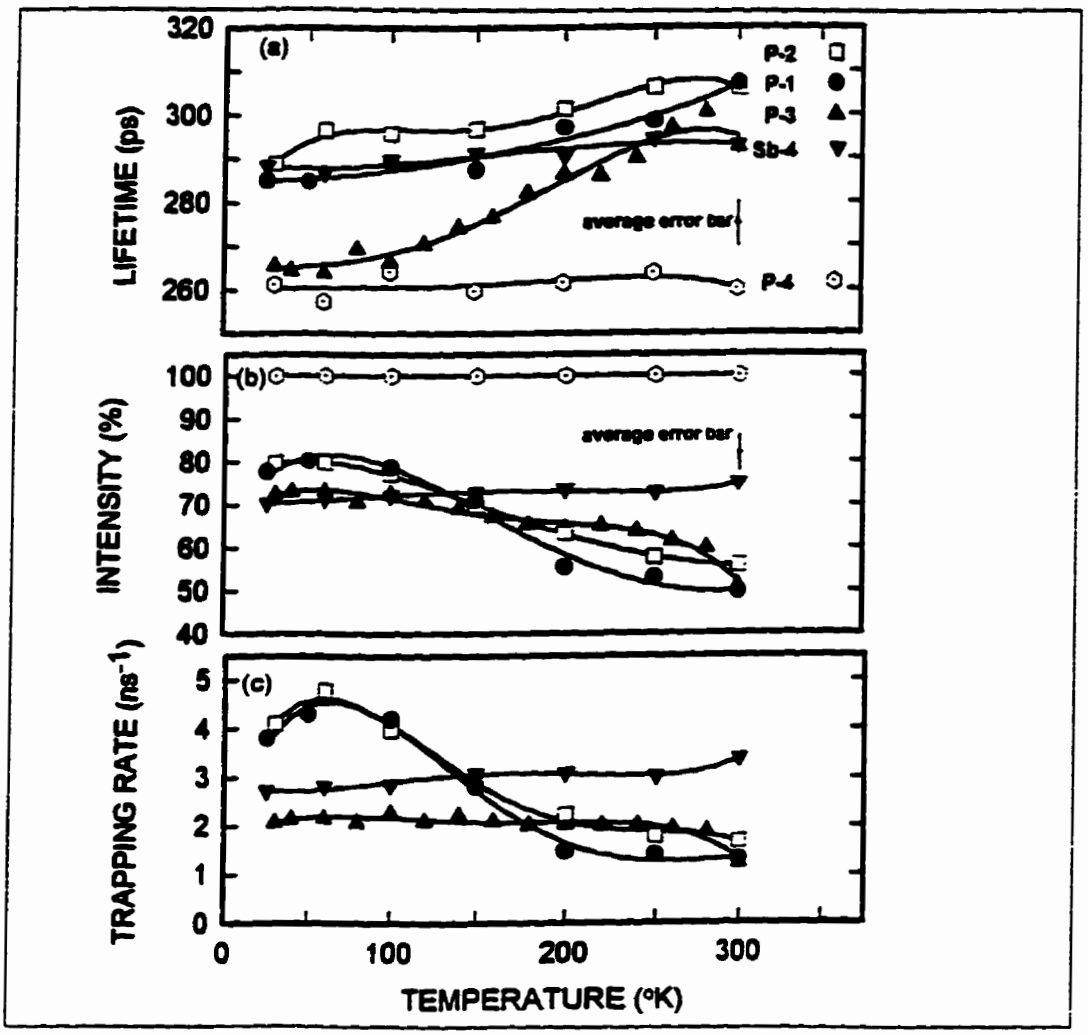

Figure 6.6. Irradiated n-type sample. Panel (a) lifetime, (b) intensity and (c) trapping rate as function of sample temperature.

Because of complete trapping, its not possible to calculate trapping rates. The medium concentration of $5x10^{17}/cm^3$ (labeled P-3) has a strong temperature dependence of the lifetime ranging between 295 ps at 300 K to 265 ps at 25 K. The trapping rate shown in figure 6.6 panel (c) is 2 ns^{-1} and temperature independent. The samples labeled P-1 and P-2 had dopant concentration of $2x10^{16}/cm^3$ and $5x10^{16}/cm^3$, respectively. They show a slight temperature dependence of the lifetime from 290 ps at 25 K to 305 ps at 300 K and the trapping rate for both materials shows a strong temperature dependence, whose behaviour is similar to the case of Fz-Si discussed earlier in section 6.2.

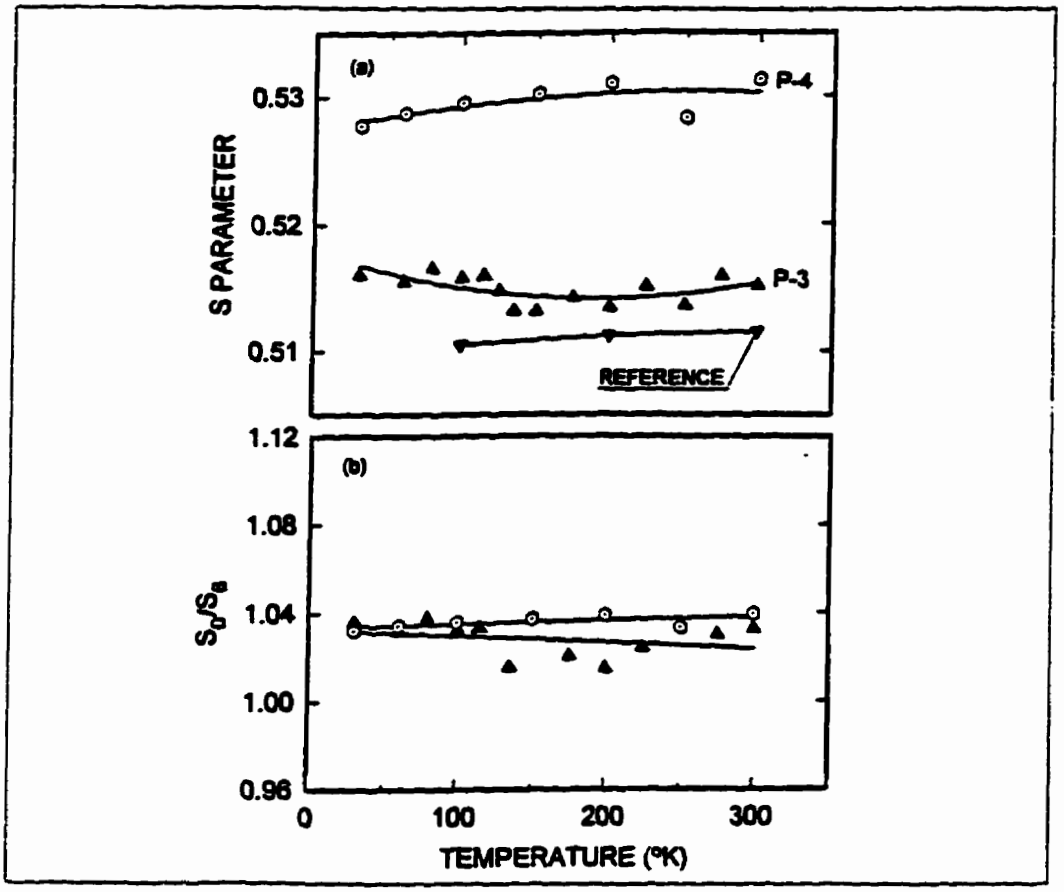

Figure 6.7 (a) Doppler S parameter for P-3 and P-4 samples. Panel (b) Defect specific S_D/S_S as a function of sample temperature.

The antimony doped, Sb-4, n-type sample presents a slight change in lifetime with temperature from 25 K to 300 K of only 5 ps, and the trapping rate of about 3 ns^{-1} is nearly temperature independent.

For samples P-3 and P-4 the doppler broadening results are shown in figure 6.7. P-4 shows an S parameter which can be consider as constant at 0.53 while P-3 has an S parameter that can be considered nearly constant in this temperature range but at a lower value of 0.514. S_D/S_B values were calculated and plotted in figure 6.7 panel (b) as function of the sample temperature and yield essentially the same values. This shows that the defect types were the same but ocurred at different concentrations in the P-3 and P-4 samples (high in the case of P-4 and lower in P-3, hence the difference in S-parameter values).

6.3.3.2 P-TYPE SAMPLES:

The results for the p-type samples, all boron doped, are shown in figure 6.8. The high concentration boron doped samples labeled B-4 with $5x10^{18}/cm^3$, presents a small variation with temperature of the lifetime from 320ps at 25 K to 300 ps at 300 K and a strong temperature dependence in the trapping rate with an *increase* of about 2 ns^{-1} in the range of 20 to 300 K. The medium concentration B-3 with $5x10^{17}/cm^3$ shows a behavior similar to that for P-3 except that the lifetime is about 15 ps lower than P-3. The trapping rate is quite small and practically temperature independent at 0.5 ns^{-1}. Finally for the low concentration boron doped sample, B-0 with $4x10^{14}/cm^3$, a small increase of 5 ps in the

range of 20 to 300 K was found, and a strong temperature dependence in the trapping rate similar to that of samples P-1 and P-2 as well as for the Fz-Si.

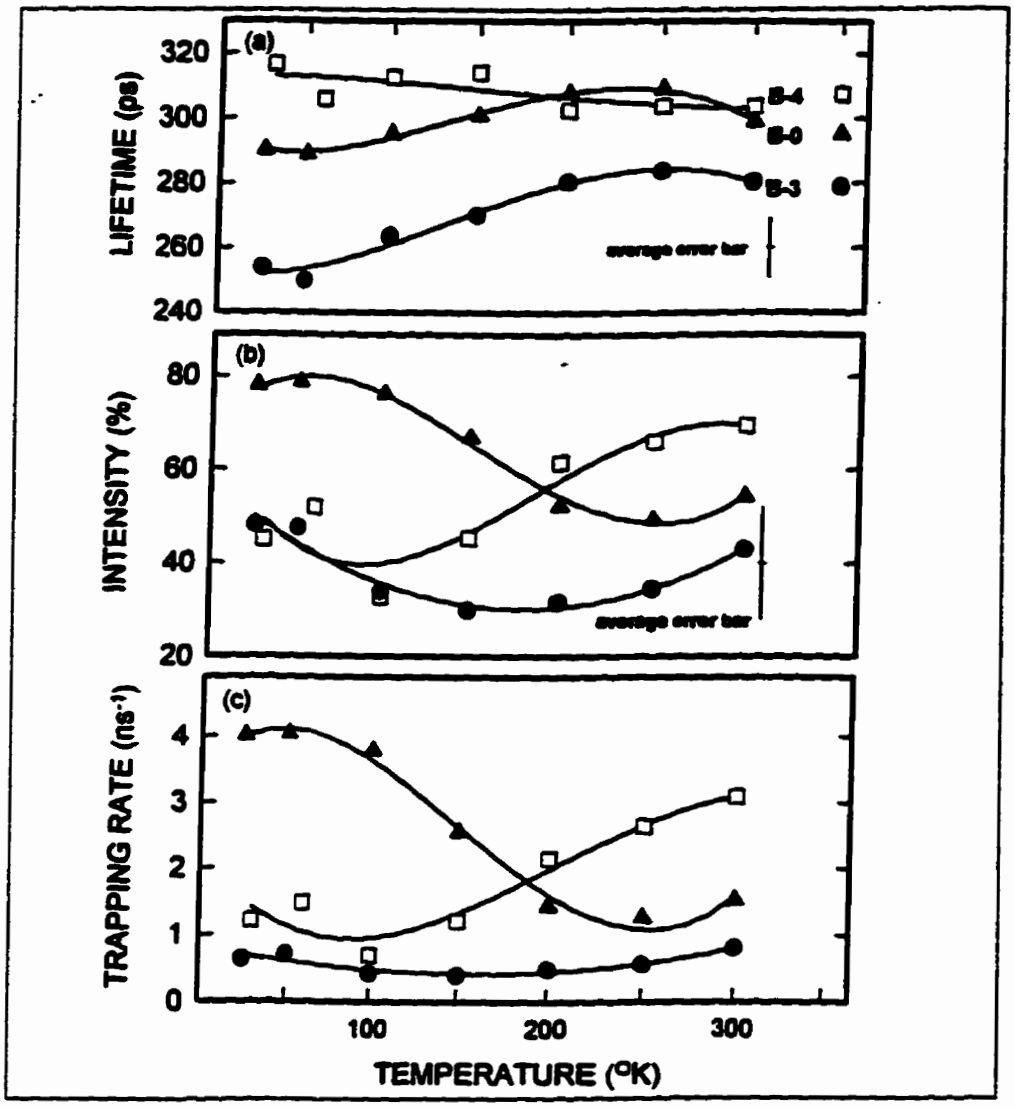

Figure 6.8 Irradiated p-type samples. Panel (a) Lifetime, (b) Intensity and (c) Trapping rate as a function of sample temperature.

6.3.4 DISCUSSION:

6.3.4.1.N-TYPE SAMPLES:

After irradiation at room temperature and high fluence, in this case 1.2×10^{18} e^-/cm^2, many monovacancies are created. At room temperature monovacancies are highly mobile, most

of them recombine with the interstitials, while others can be captured by the oxygen present in Cz-Si. Another portion of the monovacancies are trapped by the phosphorus to form VP pairs which are stable at room temperature. In the case of P-1 and P-2 samples as shown in figure 6.6 panel (a) the concentration of phosphorus is low and the amount of VP created is below the detection limit by the positron annihilation technique. In this case there is a large amount of monovacancies which form divacancies (V_2) which are stable at room temperature. For P-1, P-2 an almost constant lifetime at about 300 ps and a strong temperature dependence of the trapping rate suggest that in these Cz-Si samples the situation is the same as what found for the FZ-Si in section 6.2 of this work, i.e. the presence of oxygen has little effect.

For the P-doped material the Fermi level is initially high, so the formed divacancies could conceivably be double negatively charged even after irradiation. To check if V_2^{--} are present IR measurements were done, because V_2^{--} does not give rise to the 1.8μm band. However this absorption band was found in the P-1, P-2 which implies that the divacancies are singly charged (V_2^-).

We also noted that for P-1, P-2 the trapping rate is ≈1.8 - 2.0 ns^{-1} in contrast to ≈0.8 ns^{-1} for Fz-Si (at room temperature). Excess V_2^- are thus formed in Cz-Si by a factor of ≈2. This we ascribe to the presence of O_i, which we suggest to be active in trapping silicon interstitials so to increase the retained amount of V_2.

The P-3 sample is quite different; here τ_2 varies strongly with temperature while the trapping rate is virtually constant. In this case the concentration level of $5x10^{17}$ /cm^3 would suggest that the effect of phosphorus is dominant to form VP but also that the production of monovacancies is high enough that the phosphorus-vacancy complex can capture a second vacancy to form V_2P (phosphorus divacancy complex). This complex seems to be stable at room temperature, and this 3-body defect may have a complex structure which resembles at 300 K, an ordinary divacancy, but at low temperature more so a monovacancy VP pair. The positron may sample both vacancies at room temperature but only one at low temperature. The temperature independent trapping rate suggests this defect type to be neutral.

P-4 is a highly doped sample with a concentration of $5x10^{18}$ /cm^3. The monovacancies created by the irradiation are primarily trapped by the numerous impurities to create VP, and few, if any, V_2P complexes are formed. The concentration of VP complexes is so high that is not possible to resolve the short-lived τ_1 component for which reason the trapping rate cannot be calculated. This suggestion is reinforced by the Doppler broadening data shown in figure 6.7 panel (b) because the S_D/S_B parameter presents a constant value of 1.04 from 20-300 K.

The Sb-4 (figure 6.6) material (doped to a concentration of $1x10^{18}$ /cm^3) has a concentration about 2 times higher than P-3, and since the Sb atom is larger than the P

atom antimony is an effective trap for monovacancies. The temperature independent defect lifetime in Sb-4 is 290 ps. which contrasts with the temperature dependent 265-300 ps for P-3, but in both cases the trapping rate is nearly temperature independent. This seems to suggest that Sb has also formed neutral divacancy, but that the V_2Sb complex has only one configuration of the 3-body complex, and mainly of divacancy character.

6.3.4.2 P-TYPE SAMPLES:

Results for sample B-0 with a very low concentration of $4x10^{14}$ /cm^3 behaves (see figure 6.8) in all respects as P-1, but with a slightly lower trapping rate, $2ns^{-1}$ for P-1 and 1.5 ns^{-1} for B-0. Like before we suggest the presence of singly negative divacancies.

The B-3 sample with a concentration level of $5x10^{17}$ /cm^3 shows (figure 6.8) a behavior similar to P-3. A lower but constant trapping rate of 0.8 ns^{-1} compared to 2 ns^{-1} for P-3, can be understood by noticing that BV complexes are not stable at room temperature [73], thus it is more difficult to form BV_2 complexes. The lifetime is slightly lower than for P-3 (by 20 ps) which would suggest that the detailed 3-body configuration in BV_2 is slightly different from PV_2.

For B-4 (figure 6.8) with $5x10^{18}$ /cm^3 close to a divacancy character is observed independent of temperature in contrast to the P-4 sample which showed a monovacancy character. The BV complex is not expected to be thermally stable unlike PV, so in the boron doped sample V_2 is still the end product despite the high B concentration in contrast

to the case for high P-doping. The much higher trapping rate reflects the high B concentration. The temperature variation of the trapping rate for B-4 is singular because κ_2 increases with temperature and it appears that in the highly boron doped sample the divacancy dominates the 3-body complex rather than the mix in B-3, which is dominated by monovacancies. Further, the trapping rate for B-4 decreases with decreasing temperature, reaching approximately that of B-3 at T<100 K. We suggest that in the highly doped B-4 sample the low Fermi level renders the defects predominatly positive charged at low temperatures so few are observed. At higher temperatures holes are detrapped from the defect so more defects become neutral. This will result in an increase in the trapping rate with temperature.

6.3.5 POSITION DEPENDENCIES ALONG THE SAMPLES:

6.3.4.1 N-TYPE SAMPLES:

We calculated that the energy of the electrons at the end of the bar was about 1 MeV. This together with the fact that the amount of fluence decreases along the bar would indicate that the amount of defects created decreases along the bar. For the samples P-1 and P-2 we found mainly negative charged divacancies at the front end which received the highest radiation amount. At the other end of the bar the lifetime is slightly higher (see fig. 6.9), and the trapping rate decreases along the bar. This suggest that the fluence at the back end is still high enough to create divacancies. This is corroborated by the value of the S_D/S_B

parameter as shown in figure 6.10 which is the same as for the Fz-Si.

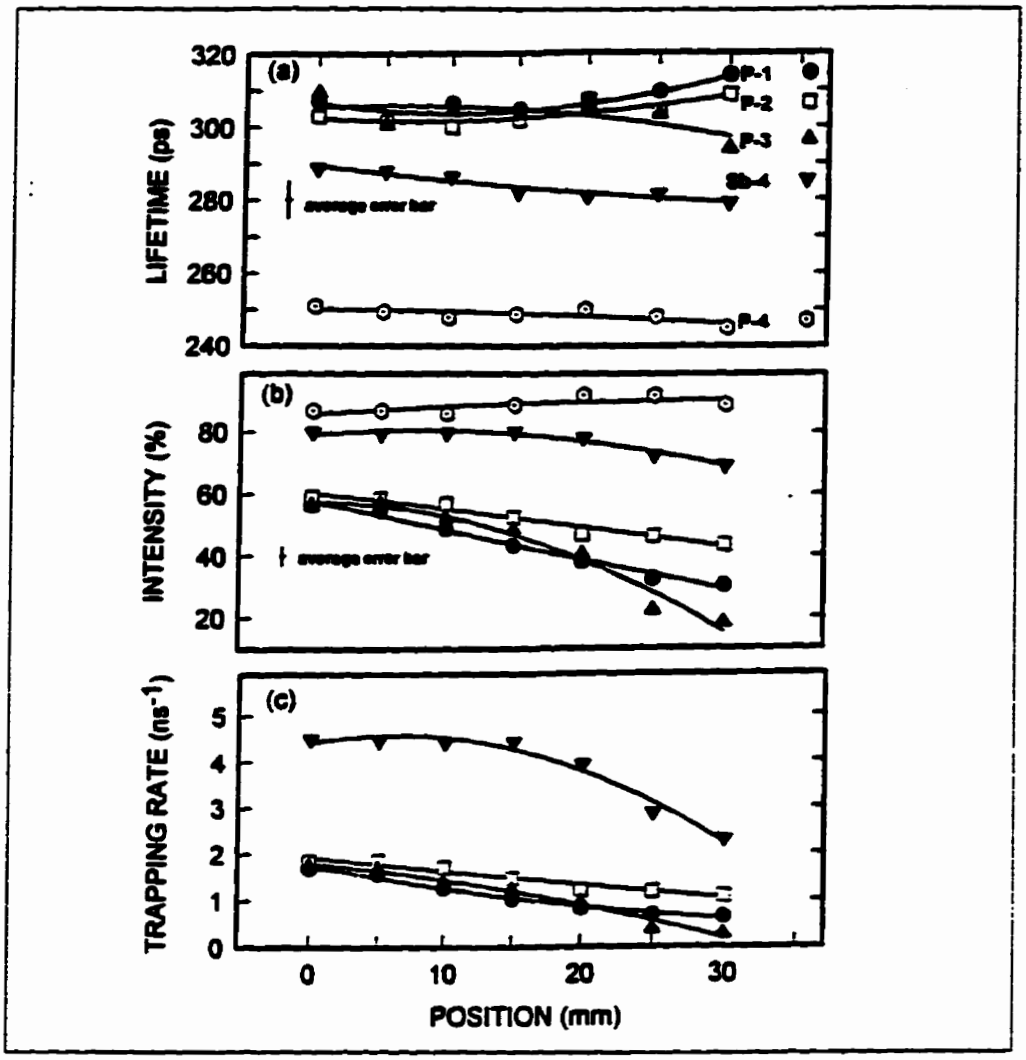

Figure 6.9 Irradiated n-type samples as a function of position.
Panel (a) lifetime, (b) Intensity and (c) Trapping rate.

In the P-3 sample, τ_2 decreases slightly with position along the bar. This is in accordance with what we discussed before, namely that lower fluence at back end of the bar will produce more PV's relative to PV_2 because of fewer monovacancies are produced in the first place, so that τ_2 will sense a larger contribution from the monovacancies trapped by the phosphorous. The κ_2 at the end of the bar is reduced to a very small amount of 0.15

ns^{-1} reflecting a lower production of defects. In qualitative agreement with the lifetime data, the S_D/S_B parameter (figure 6.10) shows a value of 1.038 for front end of the wafer and decreases to 1.02 at the other end of the bar.

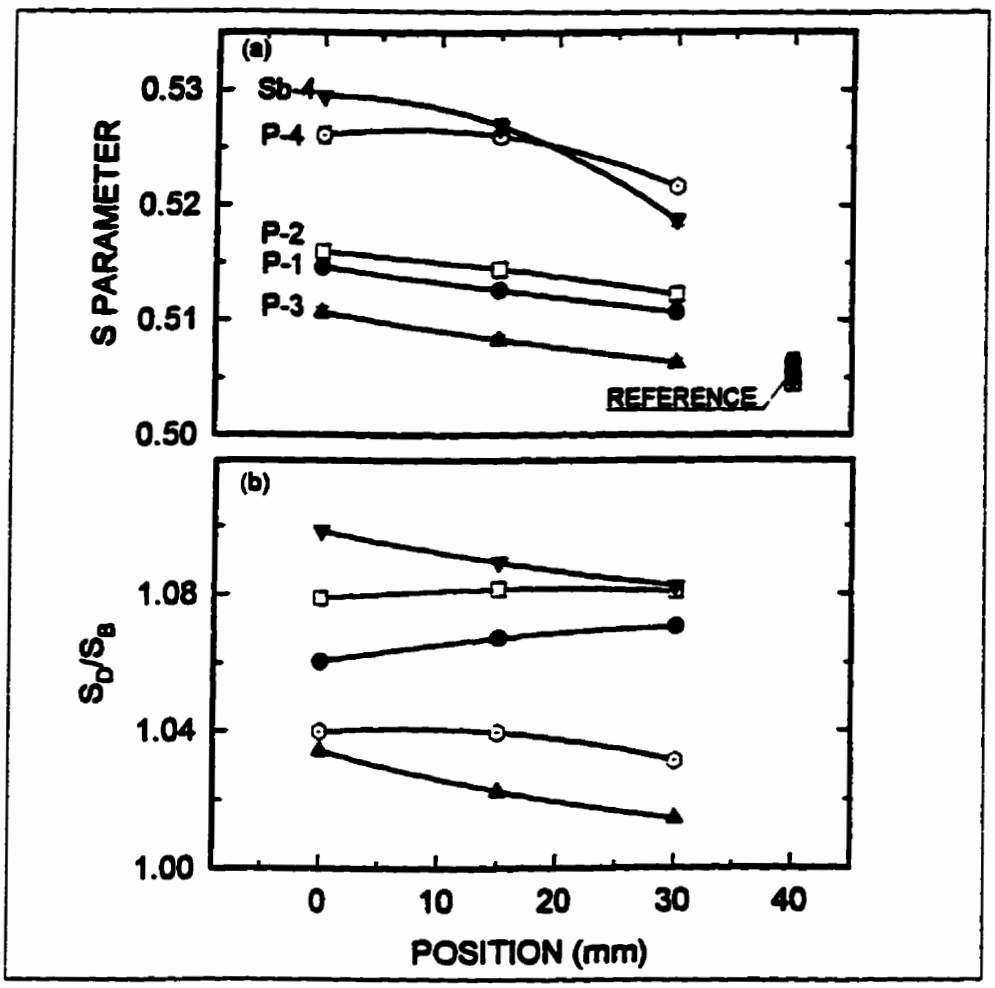

Figure 6.10 Panel (a) Doppler broadening S parameter for n-type samples Panel (b) Defect specific S_D/S_B as function of position.

For the P-4 sample τ_2 is independent on position. Here we found a dominant presence of VP's at the front of the bar, and this is the case throughout the length of the bar. Saturation trapping was found also at the end of the bar, and S_D/S_B was close to 1.04 (see figure 6.10).

For Sb-4, there is a small decrease in τ_2 from 290 at the front end to 280 ps at the back end of bar compared with the 310 ps to 300 ps found in P-3. For the front end we suggested before SbV_2 complexes. The S_D/S_B parameter gave a value of 1.10 at the front end and decreased to 1.08 at the back end of the wafer. These would suggest that a lower fluence at the back end would produced more SbV's relative to the SbV_2's. The trapping rate as function of position dropped by about 50%, which is the same amount as for the P-1 to P-3 samples. For the P-associated divacancies we note that the lifetime is essentially the same as for the free divacancies (about 300 ps). Nevertheless, the S_D/S_B values for the P-3 sample is only 1.04 whereas for the free divacancies it is 1.07. This suggest that the momentum distribution has been modified by the presence of P's. A similar effect is evident for the Sb-doped sample.

6.3.4.2. P-TYPE SAMPLES:

The results for the p-type samples are shown in figure 6.11. For the B-0 sample ($4x10^{14}/cm^3$) we found the presence of V_2^- at the front end of the bar. As a function of position, figure 6.11 panel (a) shows a slight decrease in the lifetime indicating the dominance of the V_2^- at all positions. This suggestion is reinforced by the S_D/S_B defect specific value as shown in figure 6.12 panel (b) which shows an increase from 1.06 to 1.07 for the front end of the bar, respectively, which is the same value we found for divacancies in section 6.2 of this work. The trapping rate in figure 6.11 panel (c) presents a drop from

1.5 to 0.5 ns^{-1} which reflects less defects being produced as a result of less fluence reaching the end of the bar just as in the case of the P-doped materials.

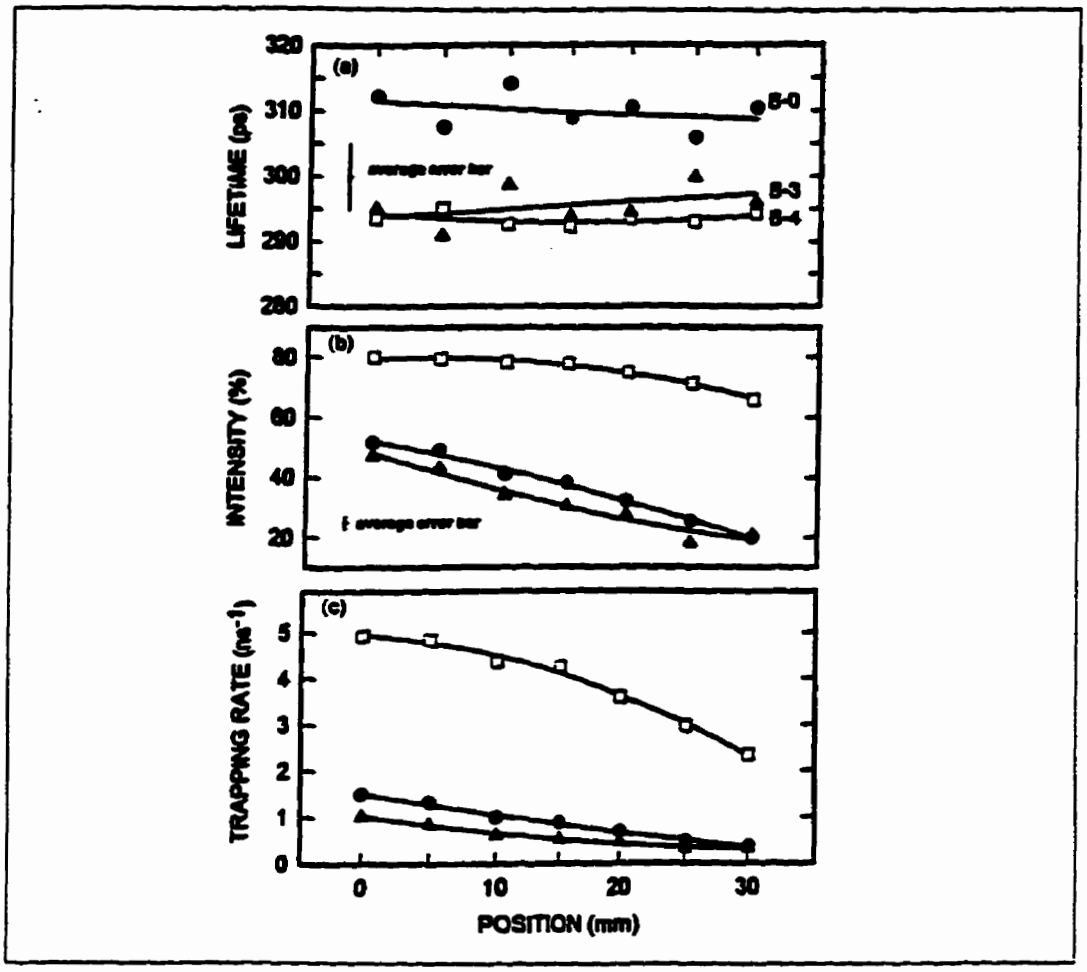

Figure 6.11. Irradiated p-type samples as function of position.
Panel (a) lifetime, (b) Intensity and (c) Trapping rate.

For sample B-3 ($5x10^{17}/cm^3$) we found BV_2-type of defects at the front end of the bar at room temperature. A constant value of 295 ps is found along the bar, suggesting that BV_2 still dominates at the back end of the bar. The defect specific value, S_D/S_B see figure 6.12 panel (b), shows an increase from 1.035 at the front end to 1.05 at the back end. The trapping rate, like before, only represents a consequence of a drop of the fluence and

therefore less production of defects.

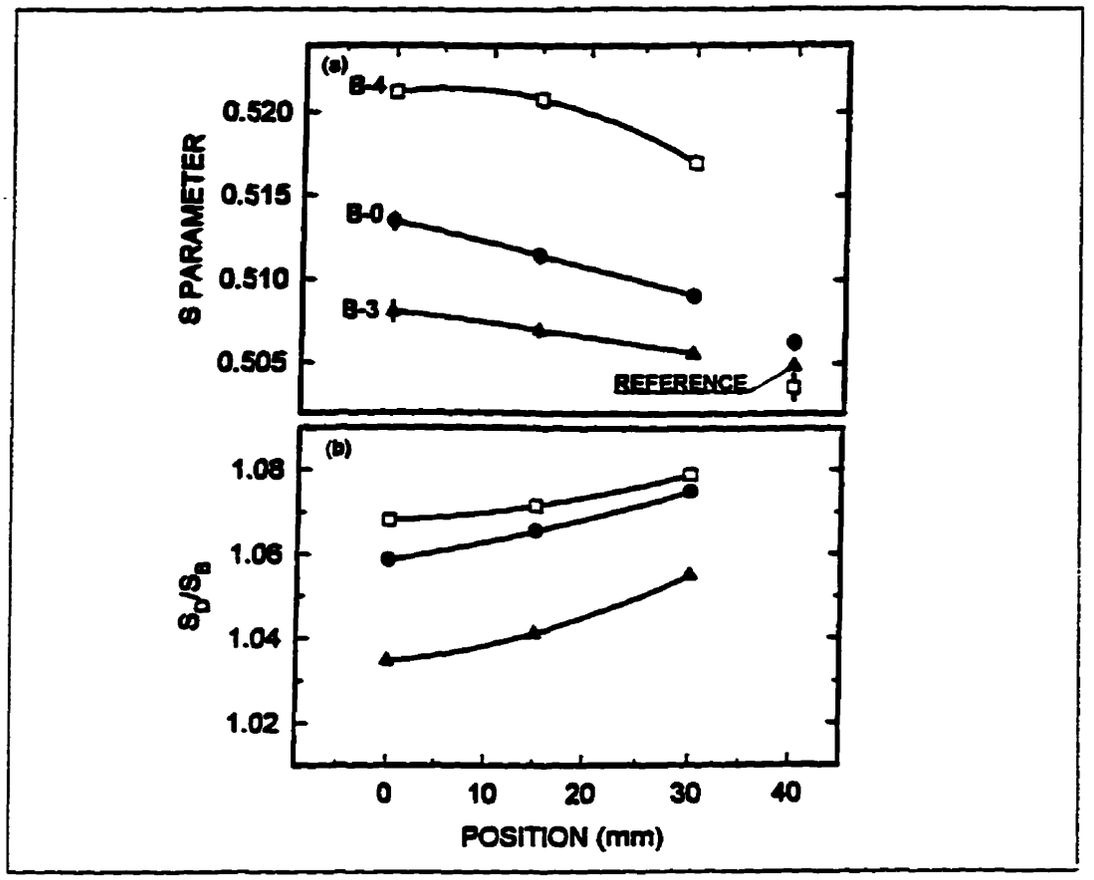

Figure 6.12. Panel (a) Doppler broadening S parameter for p-type samples. Panel (b) Defect specific S_D/S_B as function of position.

Finally for sample B-4 ($5x10^{19}/cm^3$) we concluded that V_2 is the end product despite the high B concentration (unlike the situation for the P-4 sample). The lifetime is constant at 295 ps. Based on this, we suggest that V_2 is still the dominant defect at the end of the bar, and find a high defect specific value S_D/S_B of about 1.07 to 1.08. The trapping rate like in all cases before reflects a lower fluence at end of the wafer with a less production of defects.

In the cases of the B-doped materials the positron lifetimes were all relatively closed

(295-310 ps). One would therefore have expected that S_D/S_B values also would have been closed, but this is not the case, and we suggest this to arise from the influence of the B-impurity.

6.3.6 CONCLUSION:

As a conclusion of this work, we have been able to explain most of the experimentally obtained data for the different samples. We suggested the existence of PV_2's, BV_2's and SbV_2's as possible defects present in the samples, dominating in particular at a dopant concentration of ~$5x10^{17}/cm^3$ for the dose employed in this work ($1.2x10^{18}$ e^-/cm^2). Further experimental work is necessary to confirm in more detail the defect structure, electronic level in the band gap, etc,. From the position dependencies we can conclude that the types of defects produced changed only little along the bars. The amount of defects decreased due to energy degradation and decrease in fluence by about 50%. The presence of impurities significantly modifies the Doppler S-parameter, positron lifetimes, and amount of vacancies retained after irradiation. In particular, high dopant concentrations increase significantly the amount of vacancies trapped.

REFERENCES:

1)W. Gordon. Z. Phys. 40 117 (1926)

2) P.A.M. Dirac. Proc. Cambridge. Phil. Soc. 26 361 (1929)

3) P.A.M. Dirac. Proc. Roy. Soc. A126 360 (1930).

4) C.D. Anderson, Science, New Series 76, 238 (1932).

5) C.D. Anderson, Phys. Rev. 43, 491 (1933)

6) P. Blackett, and G.P.S. Occhialini, Proc. Roy. Soc. A139, 699-726 (1933)

7) J. Tribaud, Phys. Rev. 46, 781(1934).

8) O. Klempere, Proc. Cambridge Phil. Soc. 30, 347 (1934).

9) C.I. Westbrook, D.W. Gidley, R.S. Conti, and A. Rich. Phys. Rev. A 40, 5489 (1989).

10) V.I. Goldanski. Atomic Energy Rev. 6, 1-148 (1968).

11) J. Green and J. Lee. "Positronium Chemistry". Academic Press, New York, p105 (1964).

12) B. Nielsen, "Investigation of Defects in Deformed Metals by Positron Annihilation Technique". L.F.T. II Report #2 . Lab. of Applied Physics II Technical University of Denmark p2 (1978).

13) M. Eldrup. "Positron Lifetime in Water and Ice, and in Frozen Aqueous Solutions". Danish Atomic Energy Commission, Report #254 (1971).

14) P. Hautojarvi "Positrons in Solids" Topics in Current Physics (Springer Verlag, 1979)

15) I.K. MacKenzie, I.A. Eady and, R.R. Gingerich, Phys. Lett. A 33, 279 (1970)

16) P.H. Leo, K.D. Moore, P.L. Jones, and F.H. Cocks. Phys. Stat. Sol. B 108 145 (1981).

17) EG&G Ortec Inc. Photomultiplier, Instruction Manual.

18) EG&G Ortec Inc.. Model 583 Constant-Fraction-Descriminator.. Operating and service Manual.

19) EG&G Ortec Inc. Model 566, Time-to-Amplitude-converter. Operating and Service Manual.

20) W. Puff. Appl. Phys. 18, 165 (1979).

21) P. Kirkegaard, N.J. Pedersen, and M. Eldrup: PATFIT-88, Riso-M-2740, Riso, DK--4000 Roskilde Demark.

22) P. Kirkegaard, "A FORTRAN IV Version of the Sum-of-Exponential Least-Square, Riso-M-1279, Riso, DK-4000 Roskilde, Denmark.

23) P. Kirkegaard, "Some Aspects of the General Least-Squares Problem for Data Fitting" Riso-M-1399 DK-4000 Roskilde, Denmark.

24) P. Kirkegaard, and M. Eldrup, "The Least-Squares Fitting Programme POSITRONFIT: Principles and Formulas. Riso-M-1400. DK-4000 Roskilde, Denmark.

25) S. Dannefaer, and D. Kerr, Phys. Rev. B 50 14096 (1994).

26) V. Vlack, "Elements of Material Science and Engineering" Third Edition p146 (1977).

27) M. Lannoo and J. Bourgoin "Point Defects in Semiconductors I", Solid-State Science (Springer-Verlag Berlin Heidelberg New York 1981).

28) W.E. Johnson and K. Lark-Horovitz, Phys. Rev. 76, 442 (1949)

29) G. D. Watkins. Proc. Santa Fe Conference. October 1967 Pag(67).

30) H. Rzewuski. Electron Technology 7, 39 (1974).

31) A. Kawasuso, M. Hasegawa, M Suezawa, S. Yamagushi and K. Sumino. Mat. Sci. Forum 175, 423(1995).

32) J. W. Corbett, Electron radiation damage in semiconductors and metals, Solid State Physics., Suppl. 7, (Academic Press, 1966).

33) G.D. Watkins, Proc. of the Santa Fe. Conf. on Radiation Effects in Semiconductors, (Plenum Press 1969) p67.

34) S. Dannefaer, Radiation Effects and Defects in Solids 111 65 (1989).

35) J.C. Mikkelden Jr. Mat. Res. Soc. Symp. Proc. 59 19 (1986).

36) S. Tong Lee and D. Nichols. Mat. Res. Soc. Symp. Proc. 59 31 (1986).

37) B. Pajot, and B. Cales. Mat. Res. Soc. Symp. Proc. 59 39 (1986).

38) J. Lindstrom and B.G. Svensson. Mat. Res. Soc. Symp. Proc. 59 45 (1986).

39) G.J. Bemski, Appl. Phys. 30 1195 (1959).

40) G. D. Watkins, J.W. Corbett, and R.M. Walker Appl. Phys. 30 1198 (1959).

41) S. Dannefaer, Phys. Stat. Sol. (a) 102, 481 (1987).

42) P. Sen, and C. Sen, J. of Phys. C7 2776 (1974).

43) M. Dorikens, C. Dauwe, and L. Doriken-Vanpraet, Appl. Phys. 4 271 (1974).

44) S. Dannefaer, Phys. Rev. B 14 2709 (1976).

45) W. Fush, U. Holtzthauer, S. Mantl, F.W. Richter, and R. Sturm, Phys. Stat. Sol (b) 89 69 (1978).

46) S. Dannefaer, P. Mascher, and D. Kerr, Phys. Rev. Lett. 56 2195 (1986).

47) M. Puska, O. Jepsen, O. Gunnarsson, and R.M. Niemenen. Phys. Rev. B. 34 9874 (1988).

48) M. Shimotomai, Y Ohgino, H. Fukushima, Y. Nagayasu, T. Mihara, K. Inoue, and M. Doyama. Defects and Radiation Effects in Semiconductors. Inst. Phys. Conf. Ser. #59 p241 and 679 (Institute of Physics London, 1981).

49) J.J. Kelly, and R.M. Lambrecht, Phys. Lett. 60A 475 (1977).

50) J. Makinen, C. Corbel, P. Hautojarvi, P. Moser and F. Pierre. Phys. Rev. B 39 10162 (1989)

51) P. Mascher, S. Dannefaer, and D. Kerr, Phys. Rev. B 40 11764 (1989).

52) S. Dannefaer, G.W. Dean, D. Kerr, and B.G. Hogg, Phys. Rev. B 14 2709 (1976).

53) M. Lax, Phys. Rev. B 1502 (1960).

54) H.J. Stein, J.W. Corbett, and G.D. Watkins, "Radiation Effects in Semiconductors", (Gordon and Breach, 1971).

55) M. Hirata, H. Saito, and J.H. Crawford Jr., "Lattice Deffects in Semiconductors" R.R. Hasiguti (ed) (Univ. of Tokyo Press, 1968).

56) G.D. Watkins, Phys. Rev. B 13 2511 (1976).

57) Young-Hoon Lee, and J.W. Corbett, Phys. Rev. B 13 2653 (1976).

58) J. Makinen, E. Punkka, A. Vehanen, P. Hautojarvi, J. Keinonen, M. Hautala, and E. Rauhala, J. Appl. Phys. 67 990 (1990).

59) B. Nielsen, O.W. Holland, T.C. Leung, and K.G. Lynn, J. Appl. Phys. 74 1636 (1993).

60) R.D. Golberg, P.J. Shultz, and P.J. Simpson, Appl. Surface Science 85 287 (1995).

61) R.N. West, Adv. Phys. 22 263 (1973).

62) H. Y. Fan and A.K. Ramdas, J. Appl. Phys. 30 1127 (1959).

63) L.J. Cheng, J.C. Corelli, J.W. Corbett, and G.D. Watkins, Phys. Rev. 152 761 (1966)

64) A. Kawasuso, M. Hasagawa, M. Suezawa, S. Yamaguchi and K. Sumino, Hyperfine Interactions 84 397 (1994).

65) J. W. Corbett and G.D. Watkins, Phys. Rev. 138A 555 (1965).

66) A. Kawasuso, M. Hasagawa, M. Suezawa, S. Yamaguchi, and K. Sumino, Jpn. J. Appl. Phys. 34 2197 (1995).

67) A. Kawasuso, M. Hasagawa, M. Suezawa, S. Yamaguchi and K. Sumino, Jpn. J. Appl. Phys. 85 280 (1995).

68) M. J. Puska, C. Corbel, and R.M. Nieminen, Phys. Rev. B 41 9980 (1990).

69) A. O. Evwaraye, and E. Sun, J. Appl. Phys. 47 3376 (1976).

70) R.C. Young, and J.C. Corelli, Phys. Rev. B 5 1455 (1972).

70) J. Svenson, B. Svenson and B. Monemar. Phys. Rev. B 38, 4192 (1988).

71) J. Hornstra, Philips Res. Lab. Rept. No 3497 (1959).

72) J. W. Corbett, and J.C. Bourgoin, "Point Defects in Solids", Edited by J.H. Crawford Jr. and L.M. Slifkin (Plenum, New York 1975) Vol. 2 p8-9.

73) G.D. Watkins, Phys. Rev B 12 5824 (1975).

74) V. Avalos, and S. Dannefaer, Phys. Rev. B 54, 1724 (1996).